JOURNAL OF GEOPHYSICAL RESEARCH, VOL. 94, NO. B6, PAGES 7129–7154, JUNE 10, 1989

Appalachian Stress Study 1. A Detailed Description of In Situ Stress Variations in Devonian Shales of the Appalachian Plateau

KEITH F. EVANS

Lamont-Doherty Geological Observatory of Columbia University, Palisades, New York

TERRY ENGELDER

Department of Geosciences, Pennsylvania State University, University Park

RICHARD A. PLUMB

Schlumberger-Doll Research, Ridgefield, Connecticut

We describe an experiment to measure variations in the state of stress within a horizontally bedded Devonian shale/sandstone/limestone sequence in western New York. A total of 75 stress measurements were made in three wells a kilometer or so apart using a wireline-supported hydraulic-fracturing system. The stress profiles indicate that a major drop in horizontal stress level occurs in the generally massive shales. This drop occurs principally across the lowermost member of a group of sand beds and corresponds to an offset in S_h and S_H of 3.5 and 9 MPa, respectively. Above the sands, "thrust" regime conditions prevail, although the amount by which S_h exceeds S_v is undetermined since instantaneous shut-in pressures (ISIPs) were clipped at the level of S_v due to fracture rotation. Below the sands, the regime is strike slip with both horizontal stresses showing lateral uniformity despite substantial variations in topography. The magnitude of S_h in the sand beds themselves and a lower limestone remains at least as great as S_v despite the decline in shale stress. Hence stress contrasts between these beds and neighboring shales become pronounced with depth. The contrast in S_h and S_H between the lowermost sand and the immediately underlying shale is at least 6 and 14.5 MPa, respectively. S_H levels in the lower strike-slip regime are about 1.75 times greater than S_h and are less than the value required to initiate slippage on favourably oriented frictional interfaces. For the upper thrust regime and the sand and limestone beds, however, the inferred lower bound on S_H is close to the slippage threshold for a Coulomb friction coefficient of 0.6. The orientation of S_H is ENE with a standard deviation of 20°. Fracture traces were usually splayed, occasionally spanning 30° of well bore. No systematic correlation between mean orientation and lithology is evident. Significantly different orientations were obtained for adjacent tests in which almost identical ISIPs were observed, suggesting that the fractures quickly reorient themselves to propagate normal to the least principal stress direction. Similarly, vertical traces were observed in those tests where ISIPs apparently reflect S_v, suggesting that rotation to horizontal was rapid.

INTRODUCTION

Spatial variations in the state of stress of crustal rocks in even the simplest of geological situations reflect a poorly understood interplay through time between evolving material properties and gravitational or tectonic loading conditions. Numerous other factors may influence the pattern of stress variations developed at a given locality, notably structural setting and the presence of structural discontinuities. Stress discontinuities have been observed to coincide with basement-sediment interfaces [*Haimson and Lee*, 1980], faults [*Martna et al.*, 1983; *Stephansson and Ångman*, 1986], detachments [*Becker et al.*, 1987; *Evans*, 1989], and volcanic intrusions [*Haimson and Rummel*, 1982] as well as material property variations [*Warpinski et al.*, 1983]. Yet despite the potential for complexity there can be little doubt that the pattern of stress variation contains valuable information regarding the nature of contemporary loading and those events in the rocks past which have left some imprint on an attribute of the stress distribution. If this information is to be sensibly interpreted and the physical processes governing the contemporary stress distribution better understood, it is necessary to characterize the stress variations to such a degree that whatever systematic relationships may exist between the stress distribution, material property variations, and local structure are clearly established. Through this process, it may be possible to identify the characteristic signature of those constituent mechanisms which, superposed through time, account for the observed stress distribution.

It is within the field of petroleum reservoir engineering, where knowledge of formation stresses can significantly improve the yield of hydrocarbons, that the subject of stress variations and their origin has received greatest attention [*Warpinski*, 1986]. The emphasis, however, has been to devise methods for predicting attributes of the in situ stress distribution from inexpensive surface or wireline log data, rather than to measure the formation stresses themselves [*Frisinger and Cooper*, 1985]. Attributes of particular interest are the orientation of maximum stress [*Lacy*, 1987] and the contrast in least horizontal stress magnitude between reservoir rocks and adjacent beds [*Kry and Gronseth*, 1982; *Warpinski et al.*, 1982]. Despite this commercial importance,

Paper number 88JB03448.
0148-0227/89/88JB-03448$05.00

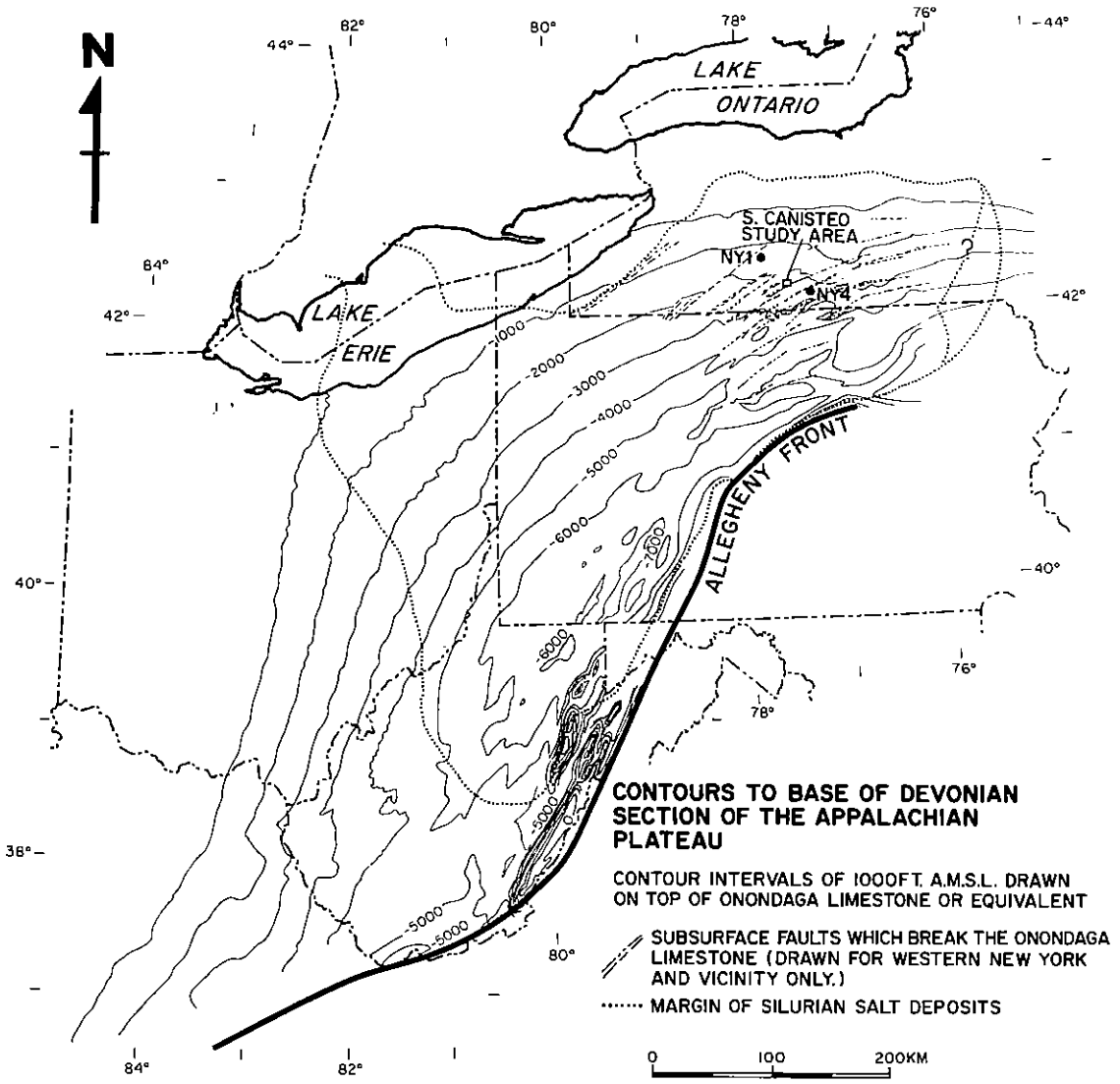

Fig. 1. Location of the South Canisteo site and nearby Eastern Gas Shale Project wells in western New York. The structural trend of the basin is defined by the contours drawn on top of the Onondaga limestone whose stratigraphic position is indicated in Figure 3. Dashed lineations in the study area signify blind reverse faults underlying anticlinal structures. The bold dotted line denotes the margin of the Silurian salt deposits.

there are few studies which feature sampling of the stress field in both the spatial extent and detail necessary to reveal clearly systematic relationships between stress and lithology. In this and companion papers we report such a study in which 75 hydrofracture stress measurements were conducted in three boreholes a kilometer or so apart which penetrate a horizontally bedded sandstone/shale/limestone sequence. This paper describes the stress measurements themselves and the pattern of stress variations that they define. Our interpretation of the observed stress variations is presented by *Evans et al.* [this issue] (hereinafter referred to as paper 2) where we provide more detailed discussion of tectonic and stratigraphic background to the study area and the results of material property analyses. The basinwide counterpart to this study is presented by *Evans* [1989]. Aspects of the measurements which have implications for the hydrofracture technique in general are dealt with more fully by *Evans and Engelder* [1989].

Background

The measurements were made in three boreholes, a kilometer or so apart, which span the side of a 230-m-high hill to the west of the village of South Canisteo in Steuben County, New York (Figures 1 and 2). The easternmost well (Wilkins 1) lies on the floor of a prominent NNW striking valley proximate to the village. The neighboring wellhead (Appleton 1) lies some 100 m up the hill a distance of 1.4 km to the WSW, and the westernmost (O'Dell) lies another 100 m higher, some 1 km due west of the Appleton.

Details of the stratigraphy of the study area are presented in paper 2. Here we mention only those features of immediate importance to the discussion of the measurements themselves. A stratigraphic cross section along the profile A-A′ of Figure 2 is shown in Figure 3. The "mechanical" base of the section of interest is formed by the extensive Salina salt deposits which serve to decouple mechanically the Devonian

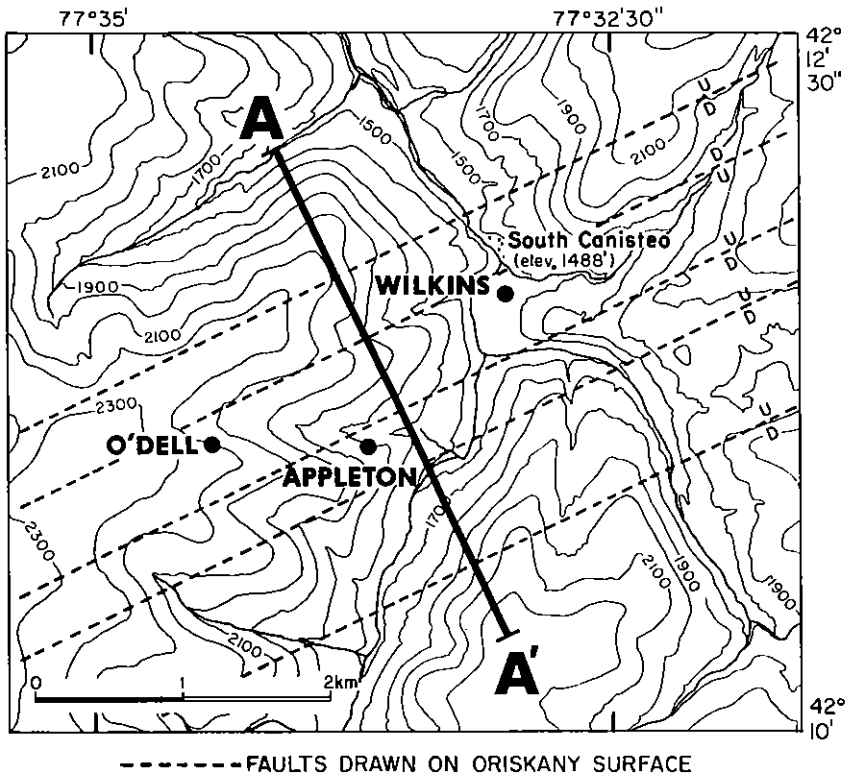

Fig. 2. Topography of the study area showing the layout of the three wells. The dashed lines show the location of blind reverse faults.

section from the underlying strata [*Evans*, 1989]. In western New York the Devonian sediments are prodeltaic and consist predominantly of alternating sequences of black and gray mudstone/siltstone turbidite piles the color of which is thought to reflect subsidence pulses associated with the Acadian orogeny [*Ettensohn*, 1985]. Below the Sonyea Group the lithology is dominantly calcareous, with the cyclical recurrence of calcareous siltstones grading upward into limestones [*Cliffs Minerals Inc.*, 1980]. Above the Sonyea, quartzitic clastics begin to appear with quartz-rich beds becoming increasingly common above the black shale base of the Rhinestreet shale. These thin (<15 m) quartz-rich beds will be referred to as sands, although in detail they are composed of intercalated beds of fine-grained sandstone and siltstone. They are widespread but rarely individually extensive on scales greater than tens of kilometers. An exception is the K-sand known locally as the Grimes sandstone which is recognized in neighboring counties. The section below the sands is cut by a family of blind reverse faults which ramp up from the Salina salt detachment. Only the larger of these northeast trending faults which show displacements of up to 15 m extend sufficiently high to cut the Tully limestone. They most likely formed in response to compression during the Alleghanian orogeny and are a common feature of decollement thrusting over salt [*Davis and Engelder*, 1985].

Field Procedures

Depth Calibration and Logging

Prior to stress testing, a borehole televiewer log was run in each well using the same trailer-based wireline as was used in the stress measurements. The objective was to identify intervals free of natural fractures for stress testing and also to calibrate the wireline depth standard against commercial natural gamma and density logs which were used to identify stratigraphic horizons of specific interest for stress measurement. Figure 4 shows the ultrasonic reflectivity imaging of a stratigraphically equivalent 30-m section of each well which spans the K-sand (Grimes sandstone). The sand can clearly be distinguished from the mudstones bounding above and below by the higher reflectivity. The capability of recognizing major bed boundaries from a log run on the same wire line as was used to lower the hydrofracturing tool was crucial in permitting precise positioning of the hydrofracturing tool with respect to the sand beds.

Owing to ease of access, the Wilkins well was selected for detailed study, and a complete suite of Schlumberger geophysical logs was run. These data and their bearing on the interpretation of the stress data are discussed by *Evans and Engelder* [1987] and *Plumb et al.* [1987].

Stress Measurement Instrumentation

Stress measurements were conducted using the wire line hydraulic-fracturing system illustrated in Figure 5. The system consists of a trailer-mounted hydraulic winch supporting 1 km of standard 7-conductor armored cable, a hydraulic high-pressure pump capable of delivering 10 L/min of water at a surface pressure of 50 MPa, and a compressor. Fluid to both inflate the downhole straddle packer and fracture the interval is delivered downhole via a single high-pressure hose clamped to the wireline every 30 m to prevent entanglement. A downhole valve operated by wire tension determines whether fluid is ported to the fracturing interval or the packers [*Rummel et al.*, 1983]. Fluid pressure is monitored downhole with a transducer (69 MPa maximum pressure and 1 part in 10^3 precision) and recorded at the surface together

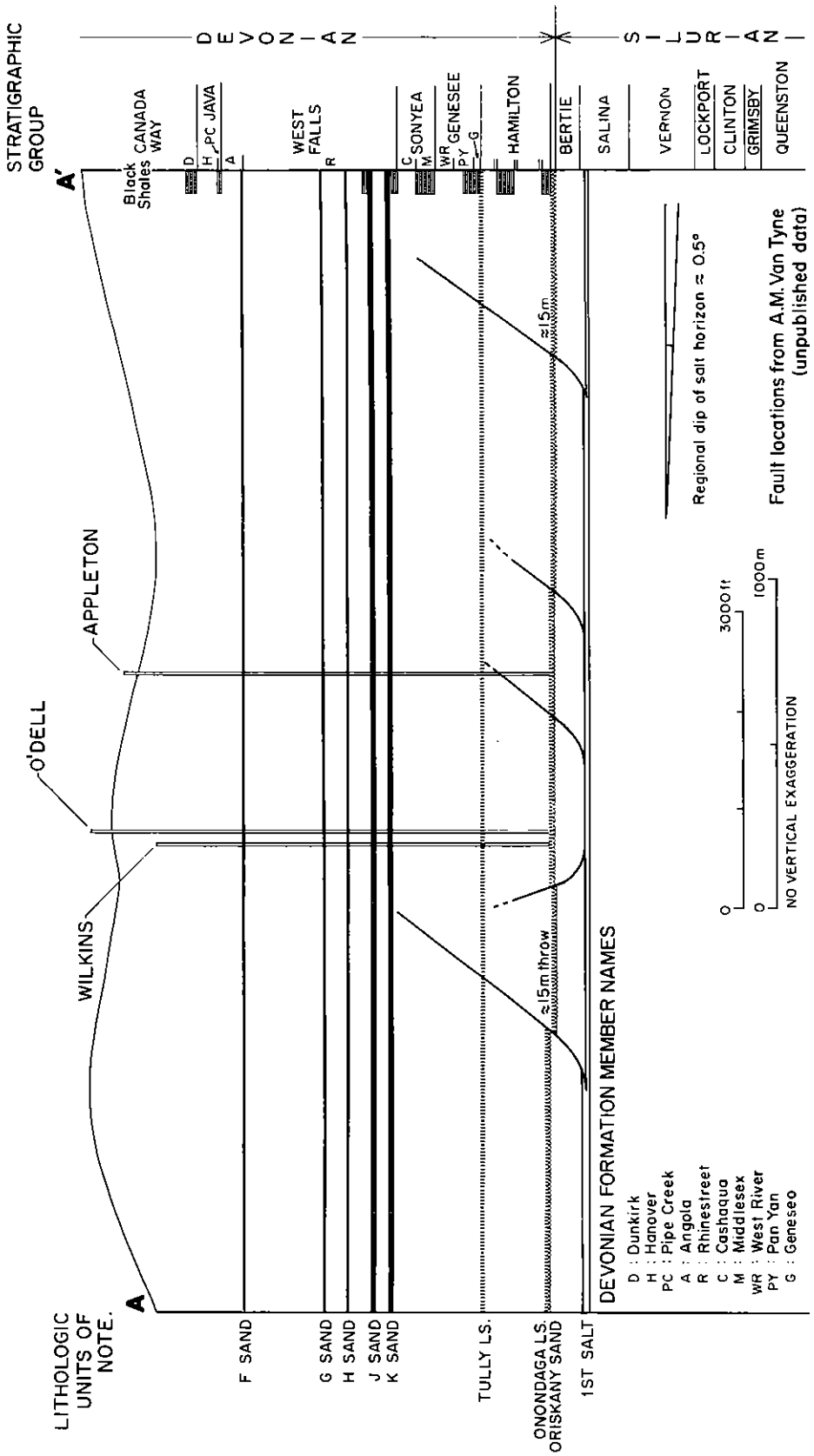

Fig. 3. Stratigraphic cross section of profile A-A' of Figure 2. There is no vertical exaggeration. The wells have been projected onto the cross section.

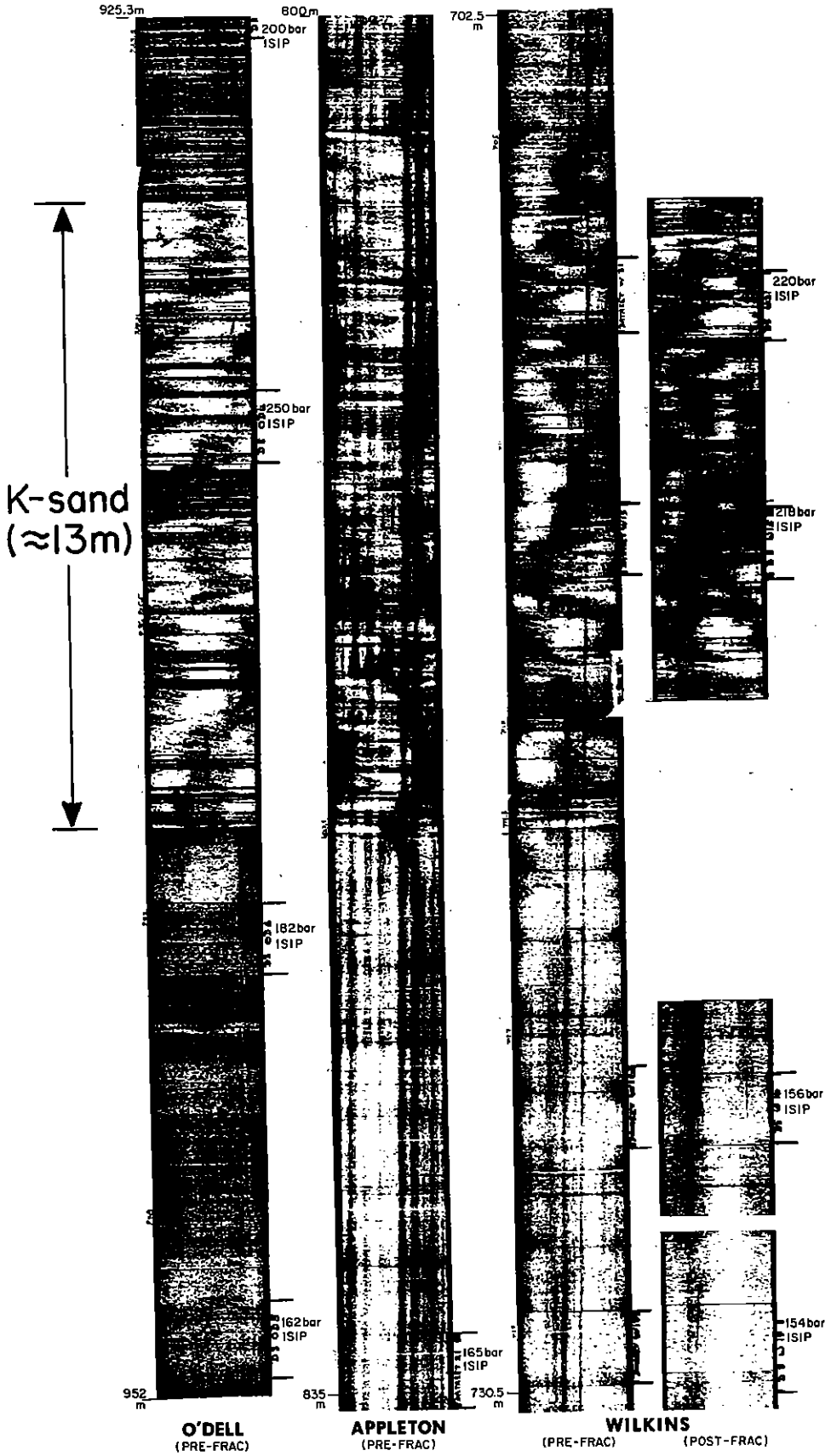

Fig. 4. Borehole televiewer reflectivity images spanning the K-sand interval in each of the three wells. Intervals stress-tested are shown together with the observed ISIP. The rightmost log was obtained following the stress testing of the Wilkins well. The traces of the induced fractures are visible in the lower intervals shown.

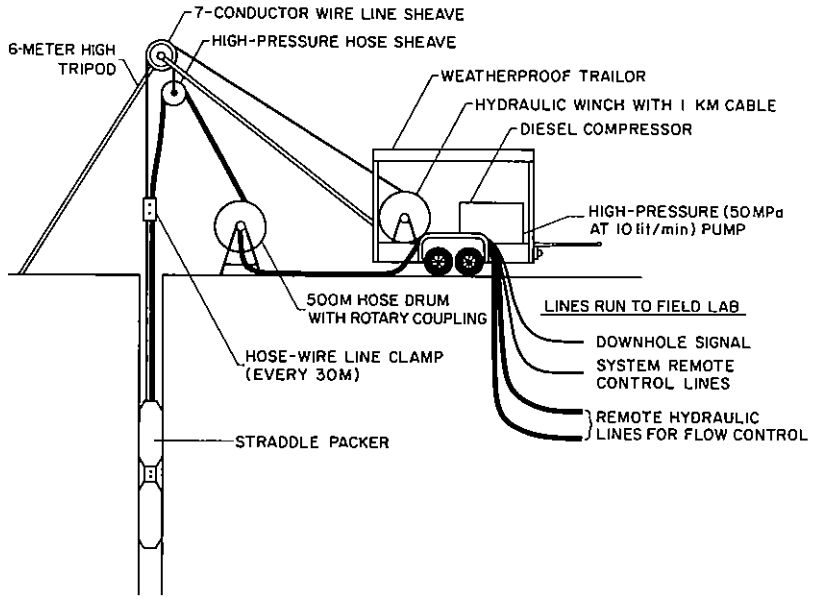

Fig. 5. Schematic diagram of the wireline "microfrac" stress measurement system used in the study.

with flow rate on strip chart and analog tape recorders. The system was developed by F. Rummel and coworkers at both Ruhr University and MESY Systems, Bochum, Federal Republic of Germany, and is identical in operation to that described by *Rummel et al.* [1983]. The straddle packer used is a standard high-pressure wash tool manufactured by TAM International of Houston, Texas. A 1.45-m straddle interval length was used in all stress tests. Packer seal length was 1.04 m. *Evans* [1987] has reported a laboratory study of the mechanical behavior of this straddle packer under conditions which simulate those encountered during the stress measurements.

Stress Measurement Technique

Upon selection of an interval for stress testing, the packers were lowered so as to straddle the interval. Precise depth control was attained through reference to color-coded marks emplaced on the wireline every 10 m and originally calibrated using a laser-ranging distance-measuring device having a standard error of 5 cm over a kilometer. A correction was applied to account for cable stretch under the weight of the tool. The packers were then inflated so as to apply a "squeeze" pressure of between 5 and 7 MPa against the borehole wall. The downhole valve was then actuated to isolate the packers and effect a hydraulic path from the high-pressure hose to the straddled interval. The interval was then ready for testing. A typical test procedure is illustrated in Figure 6 which shows the time history of downhole pressure and surface flow rate obtained during the testing of the Tully limestone interval at a depth of 1009.5 m in the Wilkins well. A permeability test was first conducted by raising the pressure in the interval by 2 MPa and monitoring the stability of the pressure after shut-in. A stable pressure was taken as confirmation that no permeable natural fractures intersected the straddled interval. Pressure was then released at the surface, and the interval pressure was allowed to fall to hydrostatic in preparation for breakdown. The pumps were then turned on full (at 10 L/min) until the attendant steady increase in downhole pressure either ceased or changed slope, thereby indicating fluid loss into a presumed induced fracture. Pumping was then abruptly stopped and the interval shut in until the pressure had stabilized. The system was then flowed back at the surface. Care was taken to monitor the volume of fluid injected and returned during all pump cycles. Flow back was interrupted periodically to monitor interval repressurization as the fracture drained pressurized fluid back into the interval. The effect of this can be seen as occasional positive jags in the pressure record during flow back periods. These jags also served to confirm that a fracture had been induced. As the rate of pressure increase during these flow back interruptions is directly proportional to the flow rate of fluid entering the interval from the draining fracture, the jags provided a measure of drainage state. Once the shut-in repressurization rate had become negligible (i.e., the fracture had adequately drained), the first reopen pump test was conducted. During this cycle, 10 L of fluid was injected, again at full pump rate, and the interval subsequently shut in and flowed back, observing the same procedure as in the breakdown pump. Once fracture drainage had again diminished to low levels, further pumping cycles were conducted involving the injection of progressively larger volumes of fluid.

During the suite of reopening pump tests, instantaneous shut-in-pressures (ISIPs) tended to decline from one cycle to the next (Figure 6). Successively larger volumes were pumped in subsequent cycles until both the injection pressure and the subsequent ISIP stabilized. The largest fluid volume injected during a single pump in any test was 100 L.

It is well known that fracture reopening pressures P_{RO} tend to decline with successive pump cycles. *Hickman and Zoback* [1983] have suggested, largely on empirical grounds, that P_{RO} measured on the second reopening cycle is the more appropriate value for maximum horizontal principal total stress S_H estimation using the method of *Bredehoeft et al.* [1976]. Although the physical processes underlying the decline in P_{RO} are not understood, inadequate drainage of the fracture pressure from the preceding pump cycle is certainly a contributing factor. To eliminate this potential

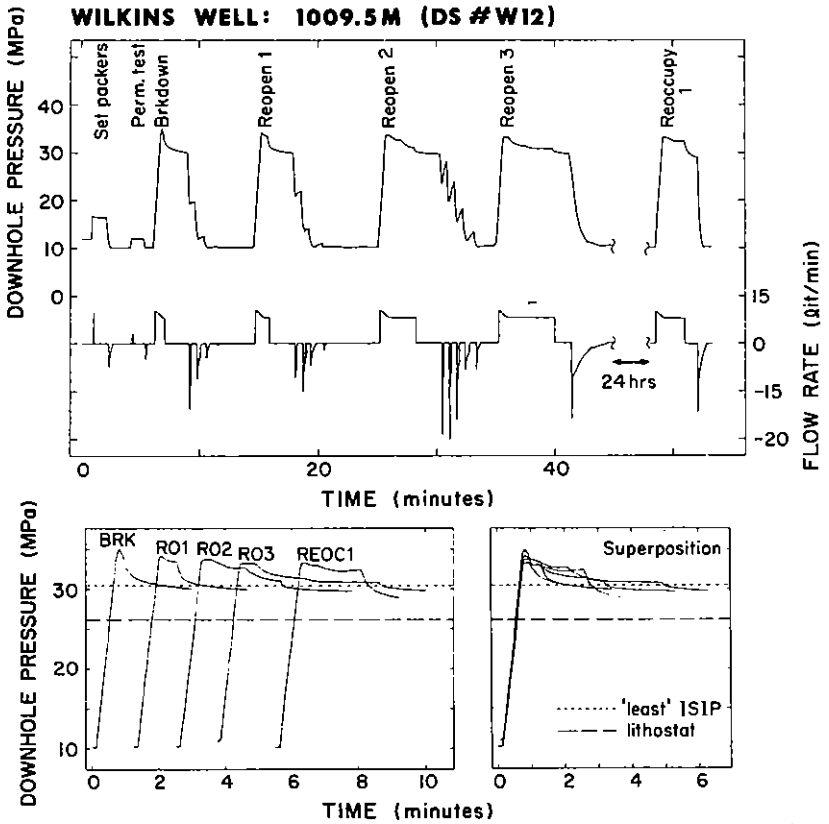

Fig. 6. Pressure and flow rate records obtained during the testing of the Tully limestone. The bottom figures are details of the top and show the pressure record written during all pumping and subsequent shut-in periods.

effect from our estimates of P_{RO}, we reoccupied 27 of the intervals tested some hours to days after performing the initial fracture sequence and conducted a "fully-drained" reopening pump test. Where an interval was not reoccupied, we used the value of P_{RO} obtained for the second reopening pump test.

The flow rates and volumes administered during a typical test are modest in comparison to those used by other workers. Calculations which assume that the induced fracture can be represented as a penny-shaped equilibrium crack in an idealized elastic medium, constrained by reasonable values of fracture toughness and elastic modulus, suggest that fracture radii of the order of 5–10 m can be anticipated using our procedures [*Evans and Engelder*, 1987]. Drainage of the fracture between pump cycles is important in limiting fracture dimensions and also in minimizing the disturbance to fluid pressures (and hence total stresses) in the vicinity of the test interval. In those cases where downhole injection pressure appeared to be limited by our modest injection rate, slow pump tests were performed to demonstrate the independence of instantaneous shut-in pressure to flow rate.

Induced fracture geometry at the well bore was determined by conducting postfracture televiewer surveys of the tested intervals. Fracture definition was enhanced by setting an impression packer against each fracture at such a pressure that the squeeze (i.e., radial stress) exerted by the packer rubber on the borehole wall was equal to the reopen pressure (to ensure that no fresh fractures were induced). The "squeeze" efficiency of the packer in question was determined from laboratory tests as 88% [*Evans*, 1987]. The fracture imaging technique proved satisfactory in 70% of cases and has the advantages of both speed and of revealing (in principle) the full extent of the induced fracture even though it may run out of the interval. This proved to be common and will be discussed later. Conventional impression packer surveys would normally reveal only the fracture trace in the interval.

RESULTS

A tabulated description of each measurement conducted including depth, lithology, pertinent pressure parameters, percentage of total pumped fluid volume returned during test and estimated stress magnitudes is presented in Table 1 for the Wilkins, Appleton, and O'Dell wells. A description of the trace of all induced fractures successfully imaged with the borehole televiewer is presented in Table 2. The discussion that follows presents graphical representations of these data.

Instantaneous Shut-in Pressures

A total of 22 intervals were stress tested in the Appleton well, 43 in the Wilkins, and 10 in the O'Dell. Instantaneous shut-in pressure was selected as the pressure at which the post-shut-in pressure decline curve departed from the linear drop defined immediately following shut-in (tangent method). A tabulation and discussion of the numerous suites of ISIPs obtained during the Canisteo tests is presented by *Evans and Engelder* [1989] and is not repeated here. In summary we note the following:

1. In almost all tests the tangent method yielded a clearly defined ISIP estimate for all reopen pump cycles. The inflection point could be determined to within 0.15 MPa. Pressure versus log time plots of several selected pressure decline curves (notably those for the Tully limestone test

TABLE 1. Description of Each Measurement

Data Point Descriptors					Measured Parameter Values					Estimated Parameter Values		
										Method 1	Method 2	
Formation[a]	Lithology[b]	Quartz Fraction, %	Data Set	Interval Depth, m	Breakdown Pressure, MPa	Reopen Pressure,[c] MPa	ISIP, MPa	Tensile Strength, MPa	Fluid, V_{in}/V_{out} (Pumps 1+2)[d]	S_H, MPa	S_H, MPa	T, MPa
						Wilkins Well						
H	S.S (D-sand)	25	W43	186.	11.5	8.05[e]	6.05	9.1 ± 4.0	0.56	13.8	8.1	3.45
H	S.S (D-sand)	35	W42	188.5	18.5	7.4[e]	6.25	9.1 ± 4.0	0.45	7.3	9.3	11.1
PC	Sil.M.S.	5	W41	194.5	35.7	9.2[e]	6.10	9.1 ± 4.0	0.65	−9.05[f]	7.0	26.5
A	S.Sil.S. (E-sand)	23	W40	198.5	26.65	7.3[g]	6.45	8.8 ± 3.0	0.77	−0.6[f]	9.9	19.35
A	Sil.S.	15	W1	203.5	21.8	9.7	6.4	8.8 ± 3.0	0.75	4.0[f]	7.3	12.1
A	Sil.S.	13	W5	207	24.8	8.55	6.7	8.8 ± 3.0	0.75	1.9[f]	9.35	16.25
A	M.S.	0	W20	252.7	22.4	10.4	7.75	8.8 ± 3.0	0.10	6.95[f]	10.15	12.0
A	Sil.S. (F-sand)	20	W21	257.2	27.4	16.75	8.1	8.8 ± 3.0	0.70	2.9[f]	4.75	10.65
R	Sil.M.S.	5	W22	266.0	27.6	13.15	7.75	8.8 ± 3.0	0.52	1.6[f]	7.25	14.45
R	Sil.S.	16	W4	342.0	19.1	13.85	10.5	8.8 ± 3.0	0.50	17.5	14.0	5.25
R	M.S.	0	W23	386.0	28.3	13.45[g]	11.45	8.8 ± 3.0	0.72	10.7	16.7	14.85
R	M.S.	0	W3	420.0	21.5	13.1[g]	13.35	8.8 ± 3.0	0.2	22.8	22.4	8.4
R	Sil.M.S.	10	W2	486.0	18.75	17.05	14.4	8.8 ± 3.0	0.58	28.0	20.9	1.7
R	S.Sil.S. (G-sand)	20	W30	501.4	21.2	18.1	15.15	8.8 ± 3.0	0.4	27.1	21.95	3.1
R	M.S.	0	W39	560.5	18.3	15.7	16.05	8.8 ± 3.0	0.3	32.65	26.45	2.6
R	M.S.	0	W14	579.	21.15	15.65[g]	17.2	8.8 ± 3.0	0.3	33.0	29.7	5.5
R	S.Sil.S. (H1-sand)	24	W10	582.5	23.7	21.3	18.2	8.8 ± 8.0	0.71	33.4	27.0	2.4
R	M.S.	2	W24	592.5	17.4	15.2[g]	16.5	8.8 ± 3.0	0.62	34.5	27.95	2.2
R	Sil.S. (H2-sand)	13	W25	597.4	24.9	19.5[e]	18.3	8.8 ± 3.0	0.25	32.35	28.9	4.4
R	Sil.M.S.	8	W38	621.8	21.1	18.3[e]	18.35	8.8 ± 3.0	0.36	37.55	31.55	2.8
R	S.Sil.S.	5	W26	652.2	17.35	15.7[g]	17.0	8.8 ± 3.0	0.42	35.4	28.25	1.65
R	S.Sil.S. (J1-sand)	17	W27	662.5	19.7	18.0[g]	20.6	8.8 ± 3.0	0.42	43.8	36.7	1.7
R	S.Sil.S (J2-sand)	13	W28	674.0	27.05	22.4[e]	20.6	8.8 ± 3.0	0.31	36.3	32.15	4.65
R	Sil.S.	9	W29	680.0	20.5	17.3[g]	19.1	8.8 ± 3.0	0.38	38.3	32.7	3.2
R	M.S.	2	W6	692.0	20.3	16.95	18.5	8.8 ± 3.0	0.65	36.5	31.1	3.35
R	S.Sil.S. (K-sand)	20	W31	707.5	21.9	22.7[g]	21.95	8.8 ± 3.0	0.6	45.1	35.5	−0.8
R	S.Sil.S. (K-sand)	15	W15	712.5	24.05	20.9	21.85	8.8 ± 3.0	0.6	42.6	37.05	3.15
R	Sil.M.S.	6	W16	724.0	19.55	15.7[g]	15.6	8.8 ± 3.0	0.23	28.2	23.3	3.85
R	Sil.M.S.	4	W17	729.0	19.4	15.8	15.4	8.8 ± 3.0	0.24	27.75	22.55	3.6
C	Sil.S.	13	W18	747.0	18.45	17.0	15.95	6.6 ± 1.2	0.20	27.95	22.8	1.45
C	Sil.M.S.	11	W37	778.15	19.4	16.9	16.05	6.6 ± 1.2	0.25	26.95	22.85	2.5
M	Sil.M.S.	17	W19	832.5	20.8	18.35	17.0	6.6 ± 1.2	0.19	27.8	23.65	2.45
M	Sil.M.S.	14	W32	840.0	19.1	17.0	16.25	6.6 ± 1.2	0.30	27.2	22.7	2.1
WR	Sil.M.S.	8	W33	860.5	25.15	17.9	17.05	7.8 ± 1.2	0.42	24.5	23.95	7.25
WR	Sil.S.	20	W9	889.5	27.25	20.45	18.5	7.8 ± 1.2	0.30	26.45	25.45	6.8
PY(b)	Sil.M.S.	13	W34	951.0	21.9	20.65	20.2	7.8 ± 1.2	0.30	36.25	29.7	1.25
PY(b)	M.S.	17	W35	960.5	23.1	20.45	20.0	7.8 ± 1.2	0.45	34.35	29.2	2.65
L	L.S.	10	W36	977.6	22.4	21.6	20.85	7.8 ± 1.2	0.27	37.4	30.4	0.8
G	M.S.	15	W7	985.5	21.7	20.9	19.9	7.8 ± 1.2	0.33	35.2	28.2	0.8
G	M.S.	15	W8	991.15	18.9	19.65	19.7	7.8 ± 1.2	0.28	37.3	28.75	−0.75
T	L.S.	0	W12	1009.5	35.05	33.3[e]	30.6	5.2 ± 3.	0.40	40.65	47.6	1.75
T	L.S.	0	W11	1013.5	26.8	25.5	24.45	5.2 ± 3.	0.39	30.45	36.95	1.3
Mo	Sil.S.	?	W13	1037.1	23.45	21.5[e]	21.8	7.8 ± 1.2	0.30	38.55	32.7	1.95
						Appleton Well						
D	Sil.M.S.		A1	186.8	25.1	6.4[g]	5.38	9.1 ± 4.0	0.66	−1.9[f]	7.65	18.7
D	M.S.		A2	230.0	21.5	7.5[g]	6.5	9.1 ± 4.0	0.69	4.6	9.5	14.0
H	S.Sil.S. (B-sand)		A3	248.5	29.5	9.25[g]	7.5	9.1 ± 4.0	0.57	−0.5[f]	10.55	20.25
H	Sil.M.S.		A4	277.5	18.0	10.5[g]	8.0	9.1 ± 4.0	0.60	12.1	10.5	6.5
H	S.Sil.S. (D2-sand)		A6	294	18.75	14.7[e]	9.0	9.1 ± 4.0	0.26	14.2	9.15	4.05
PC	Sil.M.S.		A7	305	34.8	10.9[e]	10.5	9.1 ± 4.0	0.24	2.5[f]	17.3	23.9
A	S.Sil.S. (E-sand)		A8	312	23.75	11.8[g]	10.4	8.8 ± 3.1	0.76	12.9	16.05	11.95

TABLE 1. (continued)

Data Point Descriptors					Measured Parameter Values					Estimated Parameter Values		
											Method	
Formation[a]	Lithology[b]	Quartz Fraction, %	Data Set	Interval Depth, m	Breakdown Pressure, MPa	Reopen Pressure,[c] MPa	ISIP, MPa	Tensile Strength, MPa	Fluid, V_{in}/V_{out} (Pumps 1+2)[d]	Method 1 S_H, MPa	S_H, MPA	T, MPa
					Appleton Well (continued)							
A	Sil.S.		A9	356.5	31.5	10.0[e]	10.0	8.8 ± 3.1	0.57	3.5[f]	14.4	19.7
A	S.S. (F-sand)		A10	366.0	17.85	15.5[e]	10.65	8.8 ± 3.1	0.65	18.75	12.5	2.35
R	M.S.		A11	374.25	29.2	12.85[g]	10.6	8.8 ± 3.1	0.75	7.35	14.9	16.35
R	M.S.		A12	440.7	27.55	14.9	12.5	8.8 ± 3.1	0.45	14.0	17.85	12.65
R	M.S.		A13	527.5	21.7	15.65[g]	14.65	8.8 ± 3.1	0.75	25.4	22.6	6.05
R	Sil.S.		A14	677.5	20.8	16.9[g]	18.3	8.8 ± 3.1	0.50	35.6	30.7	3.9
R	Sil.S.		A15	701.0	17.8	15.3	18.3	8.8 ± 3.1	0.49	38.35	32.05	2.5
R	S.Sil.S. (H2-sand)		A16	704.5	19.8	16.8[g]	19.2	8.8 ± 3.1	0.53	39.0	33.0	3.0
R	Sil.M.S.		A17	748.5	18.6	16.8[g]	19.2	8.8 ± 3.1	0.50	39.75	32.75	1.8
R	S.Sil.S. (J1-sand)		A18	771	25.35	21.3[e]	22.05	8.8 ± 3.1	0.50	41.3	36.55	4.05
R	S.Sil.S. (J2-sand)		A19	778.5	21.4	16.15[e]	22.05	8.8 ± 3.1	0.55	45.15	41.65	5.25
R	Sil.S.		A20	788.0	23.3	19.3[e]	20.1	8.8 ± 3.1	0.32	37.3	32.5	4.0
R	Sil.M.S.		A21	834.0	17.35	15.3[g]	15.9	8.8 ± 3.1	0.55	30.15	23.4	2.05
M	Sil.M.S.		A22	927.0	18.7	16.7[g]	16.4	6.6 ± 0.9	0.25	27.1	22.4	2.0
WR	Sil.S.		A23	1000.0	27.35	19.6[g]	19.6	7.8 ± 1.1	0.20	28.5	28.45	7.75
					O'Dell Well							
D	S.S		OD1	246.8	26.7	19.6	7.5	9.1 ± 4.0	0.2	2.25[f]	0.25[f]	7.1
D	Sil.M.S.		OD3	342.0	21.5	10.9	9.3	9.1 ± 4.0	0.75	11.8	13.5	10.6
PC	Sil.M.S.		OD2	428.3	42.2	12.5	11.4	9.1 ± 4.0	0.2	−3.5[f]	17.1	29.7
R	Sil.M.S.		OD10	864.5	31.6		20.6	8.8 ± 3.1		27.9		
R	Sil.S. (J2-sand)		OD9	896.5	52.5		24.5	8.8 ± 3.1	0.45	20.15		
R	Sil.M.S.		OD8	909.5	30.4		19.5	8.8 ± 3.1	0.3	27.1		
R	Sil.M.S.		OD7	922.5	29.2		20.0	8.8 ± 3.1	0.4	29.65		
R	Sil.S. (K-sand)		OD4	931.0	30.9		24.2	8.8 ± 3.1		40.47		
C	M.S.		OD6	942.0	44.5		18.2	6.6 ± 1.2	0.2	6.5[f]		
C	M.S.		OD5	950.2	33.4		16.2	6.6 ± 1.2		11.55		

[a]D, Dunkirk; H, Hanover; PC, Pipe Creek; A, Angola; R, Rhinestreet; C, Cashaqua; M, Middlesex; WR, West River; PY(b), Pen Yan (black shale section); L, Lodi limestone; G, Geneseo black shale; T, Tully limestone; Mo, Moscow.

[b]Log interpretations of lithology generally assume that high radioactivity and bound water content imply high clay and low quartz content and fine particle size. The percentage volume of quartz as estimated from the GLOBAL™ (mark of Schlumberger) computer-processing log is indicated. S.S., quartzitic sandstone, definition of lithology in terms of log response is low γ (80 API), neutron $\phi \leq$ density ϕ; S.Sil.S., sandy siltstone; Sil.S., siltstone, moderate γ (100–120 API), neutron $\phi \approx$ 15–20%, $\rho \approx 2.7$; Sil.M.S., silty mudstone; M.S., mudstone, high (<140 API), neutron $\phi >$20%, $\rho \approx 2.7$.

[c]Reopen pressure listed is for first reoccupation after initial fracturing pump.

[d]Average fraction of fluid returned during first and second reopening pumps.

[e]Reopen pump 2 value: greater than 3% decline in reopening pressure on subsequent pumps >0.4 MPa.

[f]Estimated value of $S_H < S_h$ and is hence not allowable.

[g]Reopen pump 2 value: less than 3% decline in reopening pressure on subsequent pumps <0.4 MPa.

shown in Figure 6) failed to reveal any features that might be taken as a higher value for the ISIP than that obtained from the tangent method.

2. As is commonly observed, ISIPs tended to decline from one pump cycle to the next, although they usually stabilized by the end of the second pump test (Figure 6). ISIPs observed in the "reoccupation" tests conducted hours to days following the initial test suite were essentially the same as the stable values obtained in the initial tests. Following the work of *Gronseth and Kry* [1983] and *Hickman and Zoback* [1983] among others, we choose the least (stable) ISIP as the best measure of least principal stress.

All tests conducted below 500 m in the O'Dell well were hampered by what appears to have been an intermittent blockage and/or leakage in the downhole apparatus. The problem manifested itself after the straddle packer had become stuck through spalled material and a pull of 2 t was applied to the wireline in order to free the tool. Although examination of the tool at the surface revealed no sign of damage, all subsequent tests yielded pressure histories which were corrupted during pumping phases. This is illustrated in Figure 7 which shows the pressure and flow rate histories obtained during the testing of the interval at 896.5 m depth. The erratic pressure variations begin as soon as the trace departs from the initial uniform pressurization rate. In Figure 7 this point coincides with the unusually stable shut-in pressure level persisting after breakdown (which was also a characteristic of the malfunction), but this was not a general rule. Following termination of pumping, the pressure histories in most cases appeared perfectly normal and yielded ISIPs which declined with successive pump cycle in the manner expected [*Evans and Engelder*, 1989]. Further-

TABLE 2. Summary of Trace Data

DS	Depth, m	Formation Member[a]	Strike of Trace, °E of N		Image Quality[b]	Extent of Trace Out of Interval, m		Direct Evidence of Bypass?[c]	Downhole Packer Pressure, MPa
			East Limb	West Limb		Upward	Downward		
				Wilkins Well					
W43[d]	186.0	H (D-sand)			5	?	?	√ (lower)	8.8
W42[d]	188.5	H (D-sand)			5	?	?	√ (lower)	9.3
W41	194.5	PC		229	3	0.0	0.0	X	9.15
W40	198.5	A (E-sand)	64?		4	0.7(?)	−0.7	X	9.45
W1[d]	203.05	A	88		3	0.96[e]	−0.75	? (upper)	7.0
W5	207.0	A		194	2	0.0	0.0	X	6.7
W20	252.7	A			5	?	?	X	8.4
W21	257.2	A (F-sand)	179?		4	−0.4	0.2(?)	X	8.6
W22	266.0	R			5	?	?	X	8.6
W4[d]	342.0	R		198	2	0.62	0.0	√ (lower)	8.4
W23	386.0	R	40	272	2	0.55	0.53	X	10.9
W3[d]	420.0	R	88	241	2	0.56	1.0[e]	√ (lower)	9.6
W2	486.0	R		268?	4	0.54(?)	0.79(?)	X	9.8
W30	501.4	R (G-sand)	29		2	0.44	0.34	X	12.5
W39[d]	560.5	R	94	274	1	0.15	0.97[e]	X	12.4
W14	579.0	R	83	272	1	0.20	0.46	X	13.4
W10	582.5	R (H1-sand)			5	0.25	−0.20?	X	11.5
W24[d]	592.5	R	66	275	2	0.41	0.0	√ (lower)	13.0
W25	597.4	R (H2-sand)		230	2	−0.30	0.35	X	13.55
W38	621.8	R			5	?	−0.20	X	13.15
W26	652.2	R	26	222	2–3	0.15	0.20?	X	14.65
W27[d]	662.5	R (J1-sand)	43 ± 35	243	2	−0.2	1.21[e]	? (lower)	14.55
W28	674.0	R (J2-sand)			5	?	?	X	15.2
W29	680.0	R	55	249	1	0.65	0.51	X	15.05
W6	692.0	R	59	239	2	0.0	0.0	X	14.8
W31	707.5	R (K-sand)		280	2	0.4	0.0	X	14.65
W15	712.5	R (K-sand)	32	249	2	0.0	0.51	X	14.65
W16[d]	724.0	R	96	275	1	0.71	1.07[e]	X	15.4
W17[d]	729.0	R	93	251	1	0.72	1.0[e]	X	15.45
W18[d]	747.0	C	64?	251?	4	0.85[e]	0.0	√ (upper)	15.4
W37[d]	778.15	C			5	?	?	√(lower)	15.9
W19[d]	832.5	M	38	281	1	0.5	1.6[e]	√ (lower)	16.45
W32[d]	840.0	M	79	190	1	1.0[e]	0.33	X	16.9
W33[d]	860.5	WR	81	261	1	0.41	1.41[e]	X	17.1
W9[d]	889.5	WR	60		2	0.78	1.0[e]	√ (lower)	14.7
W34[d]	951.0	PY	63	248	2	0.0	0.30	X	18.0
W35[d]	960.5	PY	74	254	2	0.15	1.4[e]	√ (upper)	18.6
W36[d]	977.6	L	49	266	2	0.64	1.2[e]	√ (lower)	18.5
W7[d]	985.5	G	72	250?	3	1.21[e]	1.1[e]	√ (lower)	16.15
W8[d]	991.15	G	82	249	1	1.2[e]	1.2[e]	? (upper)	16.2
W12	1009.5	T	62?		4	0.0	1.1(?)	X	16.2
W11[d]	1013.5	T	57?		4	?	?	√ (lower)	16.7
W13[d]	1037.14	Mo	75		2	1.1[e]	−0.7	X	17.2
				Appleton Well					
A1	186.8	D			5	?	?	X	11.8
A2	230.0	D			5	?	?	X	11.3
A3	248.3	H (B-sand)	85		3	−0.5	0.0	X	11.7
A4	277.29	H	85?		4	0.0?	−0.6?	X	12.3
A6	293.78	H (D-sand)	77?		4	0.0	0.0	X	12.6
A7[d]	304.78	PC	67	226 ± 39	2	0.9[e]	0.52	√ (lower)	12.5
A8	311.85	A (E-sand)			5	horiz.	horiz.	X	13.0
A9[d]	356.33	A	72	264	2	0.53	1.25[e]	√ (lower)	13.0
A10	365.83	A (F-sand)	78		3	0.0	0.0	X	13.5
A11	374.25	R			5	?	?	X	13.8
A12	440.49	R	92	272	3	0.0	0.4	X	13.8
A13[d]	527.25	R	99	295?	3	1.36[e]	0.75	? (upper)	14.8
A14	677.15	R	90?	270?	4	0.0	0.4?	X	16.7
A15	700.17	R	77	256	2	0.35	0.5	X	16.7
A16	704.17	R (H-sand)	83	291	4	0.0	0.5?	X	16.9
A17	748.14	R	85	249	2	0.0	0.9	X	17.8
A18[d]	770.64	R (J-sand)	?	328	4	?	?	√ (upper)	18.2
A19	778.14	R (J-sand)	25		3	0.0	0.0	X	18.1
A20[d]	787.63	R	178?		4	0.0	1.6[e]	? (lower)	18.3
A21	833.58	R		284	2	0.7	0.5	X	18.1
A22	926.56	M		233/297	1	0.56	0.0	X	19.15
A23	999.53	WR		244	1	0.75	0.0	X	19.9

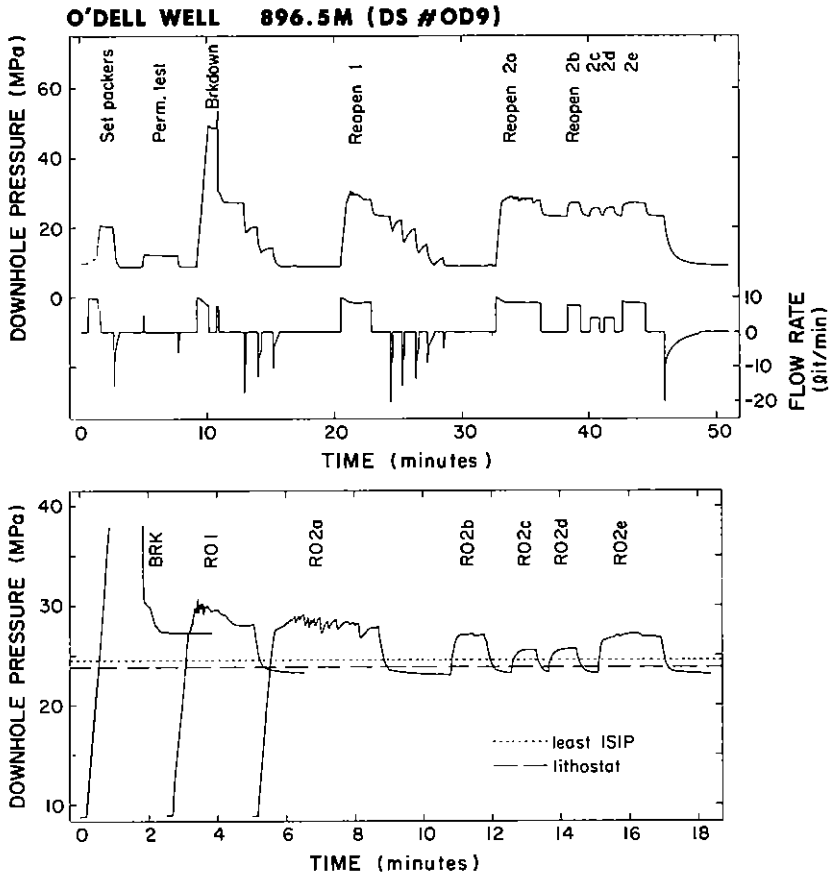

Fig. 7. Pressure and flow rate records obtained during the testing of the J2-sand in the O'Dell well. The erratic variations in pressure during pumping are most likely due to a tool malfunction. However, the shut-in pressure decline curves obtained following each pump appear to be unaffected.

more, the ISIPs showed no correlation with packer setting pressure (Figure 8). The worst affected test, DS OD4 (931 m) which was conducted immediately after pull was applied to the wireline, yielded a poorly defined ISIP of 23.7 MPa. Two subsequent reoccupations of this interval after 1 and 2 days (still with the malfunctioning tool) yielded ISIP suites of 26.5/25.0/25.0 and 24.8/24.2 MPa, respectively. In view of the seemingly well-behaved nature of the post-shut-in pressure decline and the conformance of the ISIPs to anticipated reproducible trends we accept them as measures of the least principal stress.

Depth profiles of the resulting stable ISIP values are plotted in Figure 8 for each well. The depth axes are shifted such that common stratigraphic horizons are aligned. The diagonal line represents the overburden load as estimated from a Schlumberger density log mean value of 2.71 g/cm^3. This is possibly an overestimate, as direct density measurements on core from a neighboring well (Eastern Gas Shale Project (EGSP) well NY1) suggest an average value of 2.65 g/cm^3 [*Kalyoncu et al.*, 1979]. The comparatively high density of these shallow sedimentary rocks reflects a high clay content (Figure 7 and paper 2) and the presence of calcite and pyrite. Several features of these data are noteworthy.

First, with the exception of the section between the H- and K-sands, the ISIPs define remarkably consistent linear trends showing very little scatter. Wherever closely spaced tests were performed, essentially the same ISIP values were observed. We take this as a measure of data quality.

Second, we recognize two distinct stress regimes, separated by a transition zone between the H- and K-sands. The

[a]D, Dunkirk; H, Hanover; PC, Pipe Creek; A, Angola; R, Rhinestreet; C, Cashaqua; M, Middlesex; WR, West River; PY, Pen Yan; L, Lodi limestone; G, Geneseo black shale; T, Tully limestone; Mo, Moscow.

[b]Image quality: 1, very clear trace, no vagueness; 2, clear trace of one limb, vague trace of another; 3, small segment of one trace clear, speculative infill required to estimate an azimuth; 4, trace identification somewhat speculative; 5, no trace identified.

[c]Evidence of bypass: ↓ (lower), indicates well bore below packers became pressurized during stress testing; ↓ (upper), indicates flow out of wellhead was observed during pumping; X, indicates well bore was not pressurized at end of testing and no fluid flow was observed from well bore during tests. This observation could only be made for data sets subsequent to (i.e., numerically greater than) W13 for the Wilkins and A17 for the Appleton when the static fluid head had reached the surface.

[d]There is evidence from either fracture trace length or well bore pressurization that fluid bypass of packer seals may have occurred.

[e]Potential breach of seal: fracture trace appears to extend more than 0.85 m along the 1.04-m packer seal length.

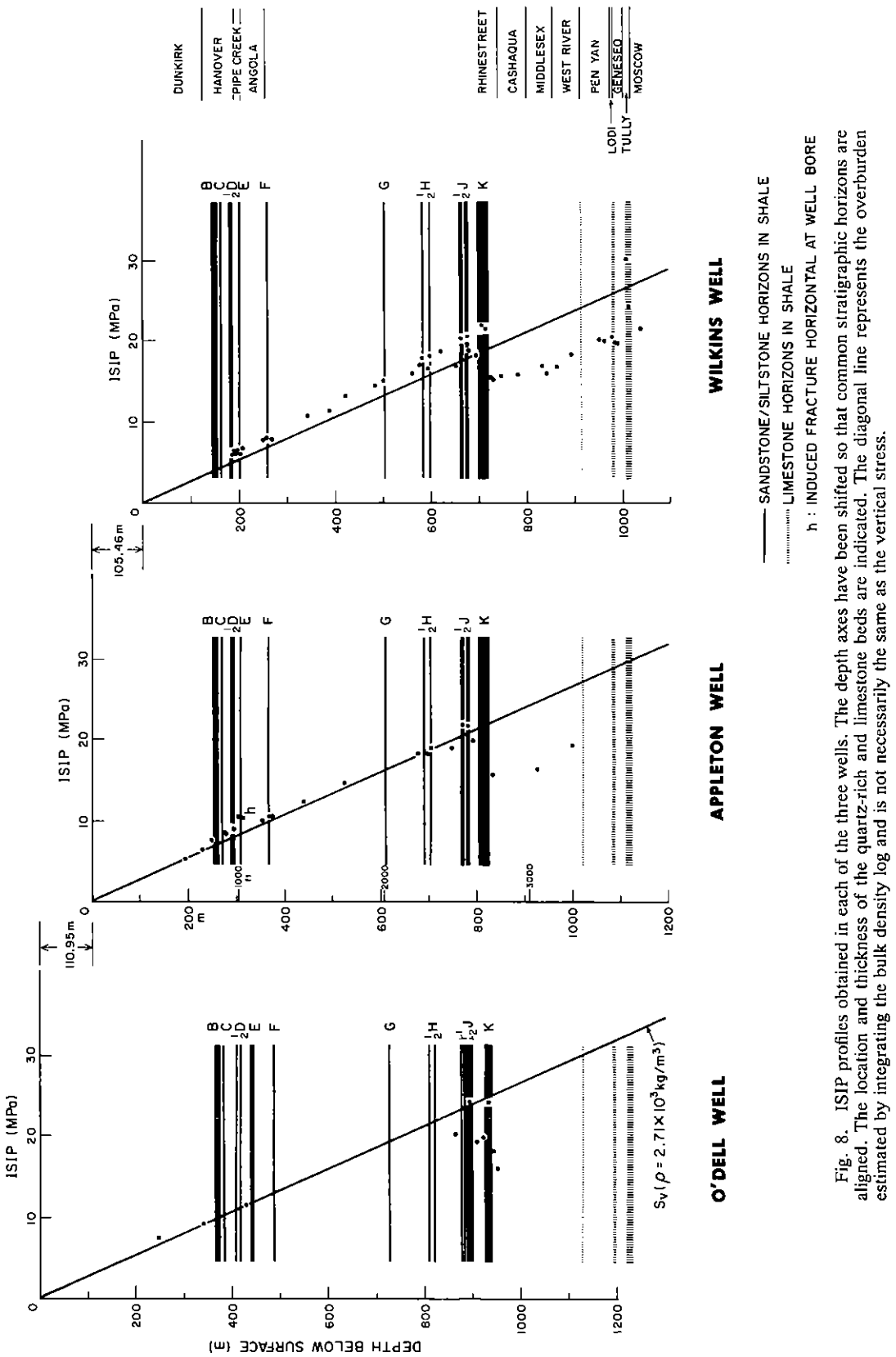

Fig. 8. ISIP profiles obtained in each of the three wells. The depth axes have been shifted so that common stratigraphic horizons are aligned. The location and thickness of the quartz-rich and limestone beds are indicated. The diagonal line represents the overburden estimated by integrating the bulk density log and is not necessarily the same as the vertical stress.

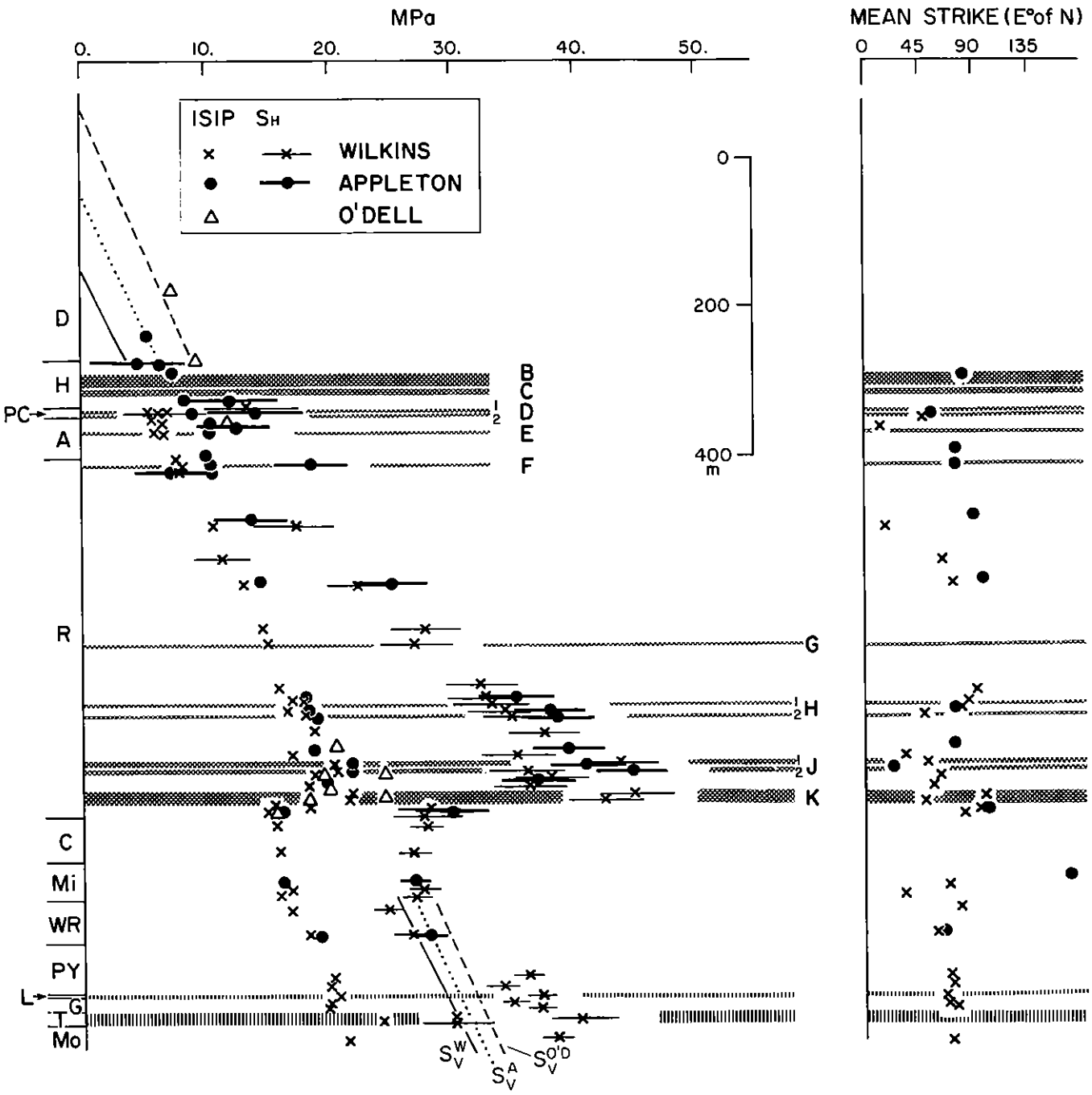

Fig. 9. Superposition of ISIPs from all three wells on a common stratigraphic section. Also shown are estimates of maximum horizontal stress calculated using method 1 subject to the assumption that ISIP is equal to the least horizontal stress. The error bar reflects the uncertainty in tensile strength. The diagonal lines correspond to the near-lithostat trends in each well which we believe denote the vertical stress.

upper regime is characterized by ISIPs which lie on or marginally above the overburden trend for each well. Specifically, for the O'Dell, Appleton, and Wilkins wells the ISIPs increase linearly with depth at a rate which exceeds the density log derived overburden gradient by a factor of 1.0, 1.07, and 1.16, respectively. Henceforth we refer to these trends as the "near-lithostat trends." As the wellhead heights differ by up to 213 m and bedding is essentially horizontal, the ISIPs measured at a given stratigraphic horizon in the upper regime vary significantly from well to well. In contrast, the lower regime, extending below the K-sand, is characterized by ISIP values substantially less than the overburden. Moreover, at a given stratigraphic horizon, the ISIPs are essentially the same in each well, irrespective of the different overburden loads. This is evident in Figure 9, where we show a superposition of all data plotted according to stratigraphic depth, and in the detail to Figure 9 presented in Figure 10 (note that the diagonal lines in Figure 9 represent overburden, whereas those in Figures 9 and 10 represent the near-lithostat trends). This constancy suggests a subsurface horizontal stress regime which is laterally uniform on a scale of at least several kilometers.

Third, we recognize a transition zone between the upper and lower stress regimes which extends from the H- to the

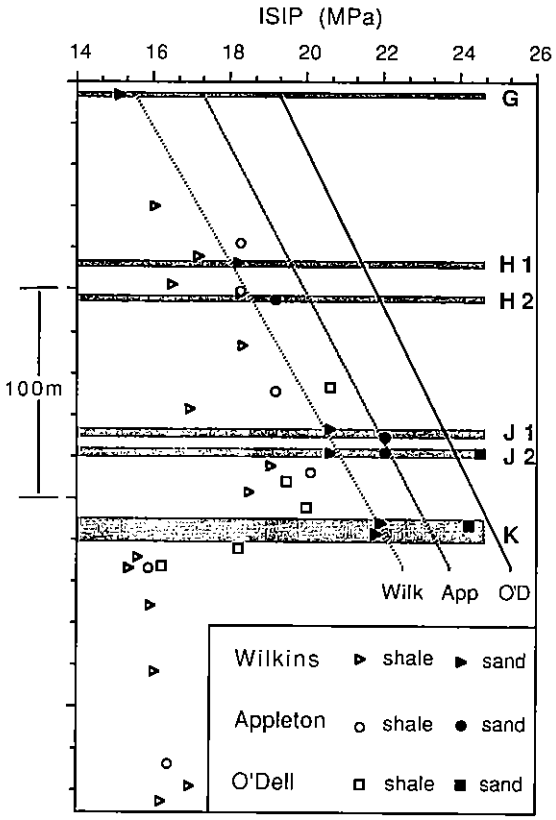

Fig. 10. Detail to Figure 10 showing the stratigraphic variation in ISIPs observed in the vicinity of the transition zone.

K-sands (Figure 10). Within this zone, ISIPs measured in the quartz-rich siltstone beds remain precisely on the near-lithostat trends established in the upper regime of each well, whereas ISIPs measured in the "shales" fall significantly below the appropriate trend by an amount which generally increases with depth. The pressure and flow rate (injection only) records obtained during the testing of the K-sand and the immediately underlying shale in the Wilkins well are shown in Figure 11. The location of both these intervals (DS W15 and DS W16) is shown in Figure 4. The difference in pumping pressures (~6 MPa) is remarkable considering the intervals are only 10 m apart. Similarly, in the O'Dell well, systematic contrasts in ISIPs between both K- and J-sands and the intervening shale attain a value of 5 MPa. At greater depth we find one ISIP measured in the Tully limestone also lies close to the near-lithostat trends (Figure 8; note diagonal lines represent overburden) and contrasts strongly with those measured in the adjacent shales.

Fracture Trace Geometry

Owing to time constraints, postfracturing televiewer surveys were conducted in only the Appleton and Wilkins wells. In 70% of cases it was possible to identify a new trace of sufficient extent and clarity to determine sensibly the strike and vertical extent of the induced fracture(s). Sketches of the identified fracture traces as they appeared in the postfracturing televiewer survey are presented in Figure 12. A dashed trace indicates that recognition was uncertain. Table 2 gives a summary of the image data for the Wilkins and Appleton wells. Here we note the following:

The vast majority of the fractures were determined to be within 10° of vertical. The only clear exception was the fracture induced at the H-sand horizon (311.85 m) in the Appleton well which was determined to be horizontal. It is generally difficult to recognize horizontal fracture traces in strongly bedded formations, and it is not possible to discount their presence on the strength of the televiewer images alone. The principal evidence that they were not common arose from our practice of setting an impression packer in each interval for 30 min prior to the televiewer survey. Upon returning the packer to the surface after having "pressed" the uppermost 11 induced fractures in the Appleton well (except the interval at 311.85 m), the rubber was found to be decorated with vertical fracture traces with no horizontal traces evident.

The inferred mean strikes of the vertical fracture limbs from the Wilkins and Appleton well surveys are shown in Figures 13 and 14, respectively. The data are segregated into successive 200 m depth groupings. Fractures induced in the quartz-rich beds are indicated by dashed lines. In several cases only one fracture limb could be identified. This should not be taken to imply uniaxial fracture propagation from the well bore as it may be due to limited televiewer resolution.

Bilateral fractures were rarely straight and 180° opposed. Rather, there was a strong tendency for bifurcation, the splays occasionally spanning 40° of well bore. Where splaying was observed, the orientation of the limbs shown in Figures 13 and 14 represents the mean value.

A large degree of scatter in limb orientation is evident. Some of this can be ascribed to instrumental error. Our experience in running three different televiewer tools during the surveys, often with multiple passes of the same interval, led us to conclude that image orientation varied in a seemingly nonsystematic manner at the level of about ±7° from magnetic north. This was found even for the same tool imaging the same interval on different days. Even allowing for this, however, the scatter in orientation is surprisingly large, given the smooth variation in ISIPs. Using the circular statistical methods of *Mardia* [1972], we find a mean orientation of N68.5°E (true) for the Wilkins and N80°E for the Appleton, the standard deviations being 24° and 23°, respectively. In Figure 9 we have plotted mean strike alongside the corresponding stress estimates (see also Figures 17 and 18). For bilateral fractures it was assumed that the two traces represent the expression of a single planar fracture that intersects the well bore, not necessarily diametrically. Unlike the stress magnitudes, no systematic first-order correlation with lithology is evident in the stress transition zone. Furthermore, outside of this zone, the scatter in orientation is not reflected in the inferred stress magnitudes which define smooth consistent trends. From this we conclude that the scatter largely reflects the distribution of flaws which serve as fracture initiation points and that the fractures tend to align themselves with the maximum stress direction after propagating some short distance from the well bore. Similar scatter in well bore fracture orientation has been reported by *Overbey and Rough* [1968] for induced fractures in sandstones equivalent to our B-sand in a neighboring county.

DATA ANALYSIS

Interpretation of ISIPs

As the televiewer imaging indicates that almost all induced fractures were vertical at the well bore, it might seem justifiable to follow convention and interpret the ISIP values as direct measures of the least horizontal principal stress S_h. This is

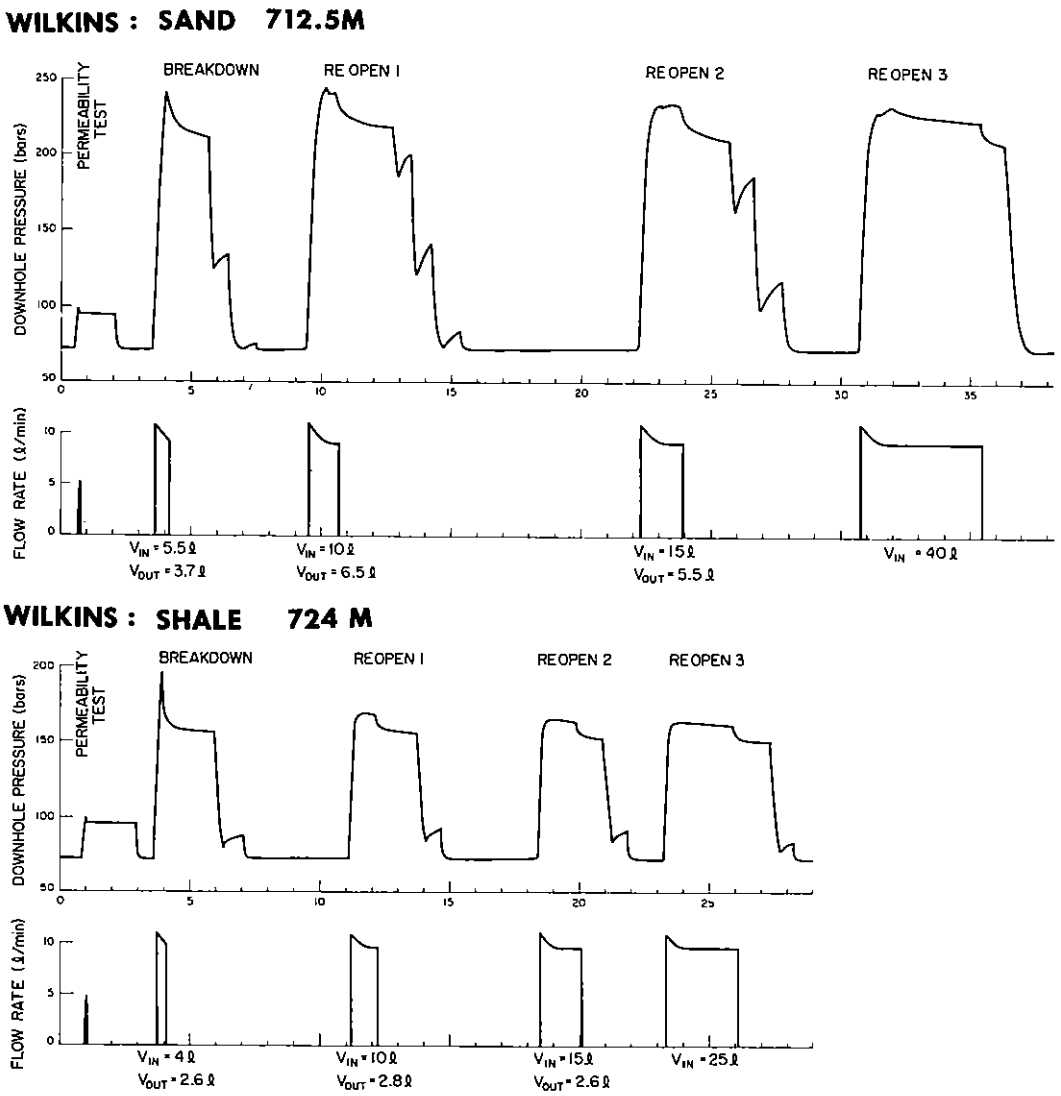

Fig. 11. Pressure and injection rate records obtained during two tests; one conducted in the K-sand and the other in the immediately underlying shale. Note the difference in pumping pressures even though the intervals are only 10 m apart (see Figure 4).

certainly reasonable for the lower regime where ISIPs are significantly less than the anticipated vertical stress. However, in situations where the measured ISIPs correspond closely to the overburden, as in the upper regime, convention must be treated with caution. For then there exists the possibility that the least horizontal stress may exceed the vertical stress by an arbitrary amount and thereby have induced the fracture to turn from vertical to horizontal as it propagated from the well bore [*Warren and Smith*, 1985], resulting in an ISIP that reflects the vertical stress [*Zoback et al.*, 1977]. In such circumstances the ISIP will provide only a lower bound to the true value of S_h which will remain otherwise undetermined. This poses a question for the interpretation of those ISIPs which fall close to the near-lithostat trends. Do they reflect least horizontal stress magnitudes or do they reflect vertical stress? In situations where significant topography exists and stress measurements from several neighboring boreholes with wellheads at different elevations are available, it is possible, in principle, to decide which is the case through examination of the spatial variation of the three-dimensional ISIP distribution. Since the wellheads at the South Canisteo site differ in elevation by up to 200 m, the data are well suited to this form of analysis. A detailed discussion of the modeling is presented by *Evans and Engelder* [1989]. In summary of the results and their bearing on the interpretation of the near-lithostat ISIPs we note the following:

Below a few hundred meters depth, the influence of topography on the lateral variation of vertical stress is much more pronounced than on the lateral variation of the horizontal stresses. This is illustrated in Figure 15 which shows contours of valley-normal horizontal stress and vertical stress predicted to result from the erosion of a symmetric valley into a laterally confined half-space. The model is from *Savage et al.* [1985] and assumes plane strain conditions and a Poisson's ratio of 0.33. All stress magnitudes are normalized by $\rho g b$, where b is the depth of the valley floor below the plateau top, here equal to 213 m. The upper and lower pair of figures correspond to different theoretical topographic profiles defined by the bold line at the surface of the eroded half-space. A two-dimensional approximation of the mean topographic slope in the immediate vicinity of the Wilkins and Appleton wells is shown for comparison. Further details are given by *Evans and Engelder* [1989] and *Savage et al.* [1985]. The important point is that the

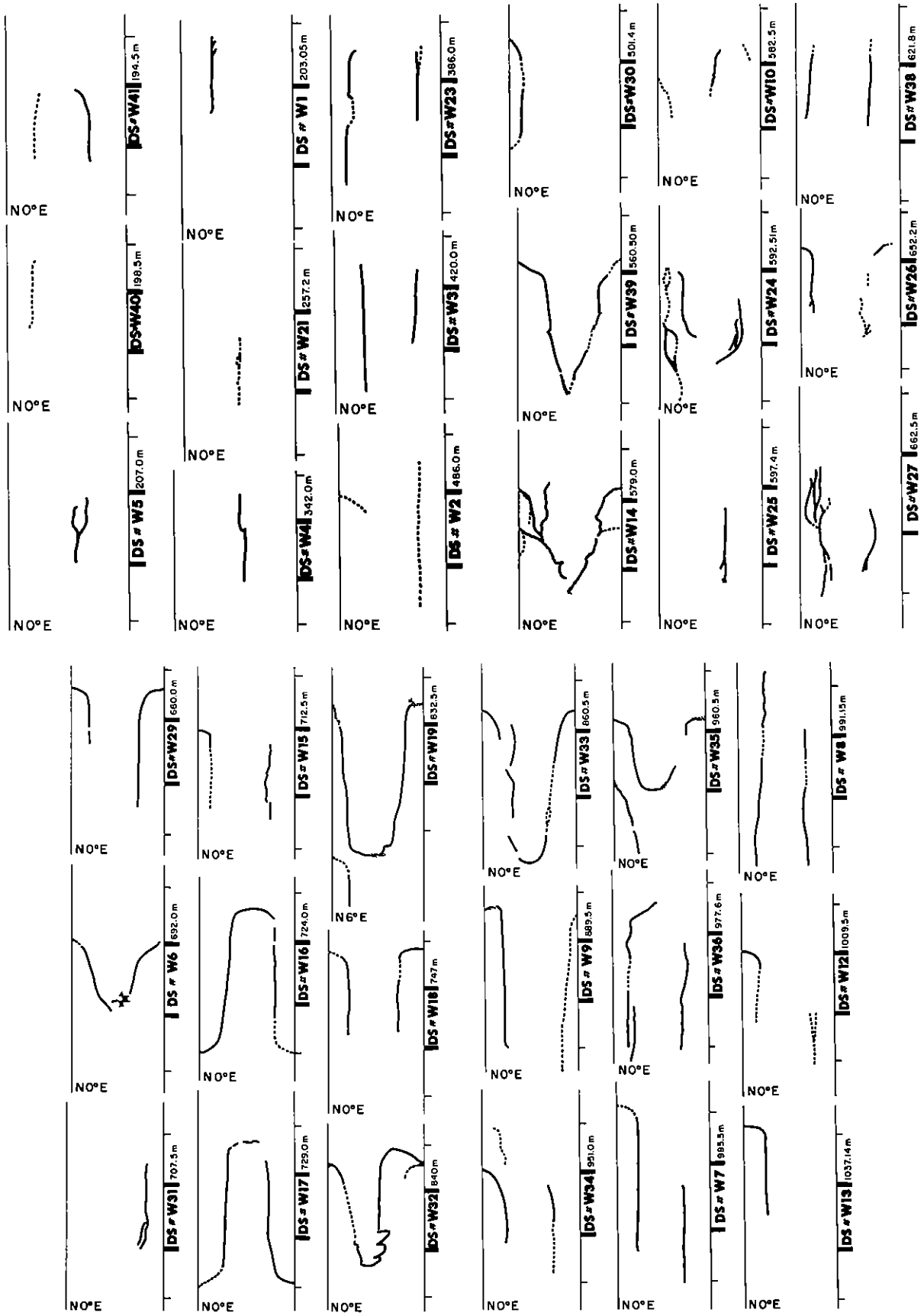

Fig. 12. Sketches of induced fracture trace geometry. A dashed trace indicates that identification is uncertain. For each diagram the section of borehole pressurized lies between the two bold lines bounding the "data set number." The outer solid lines indicate the upper and lower extent of the packer seals. The orientation of the left margin of each trace is given with respect to magnetic north.

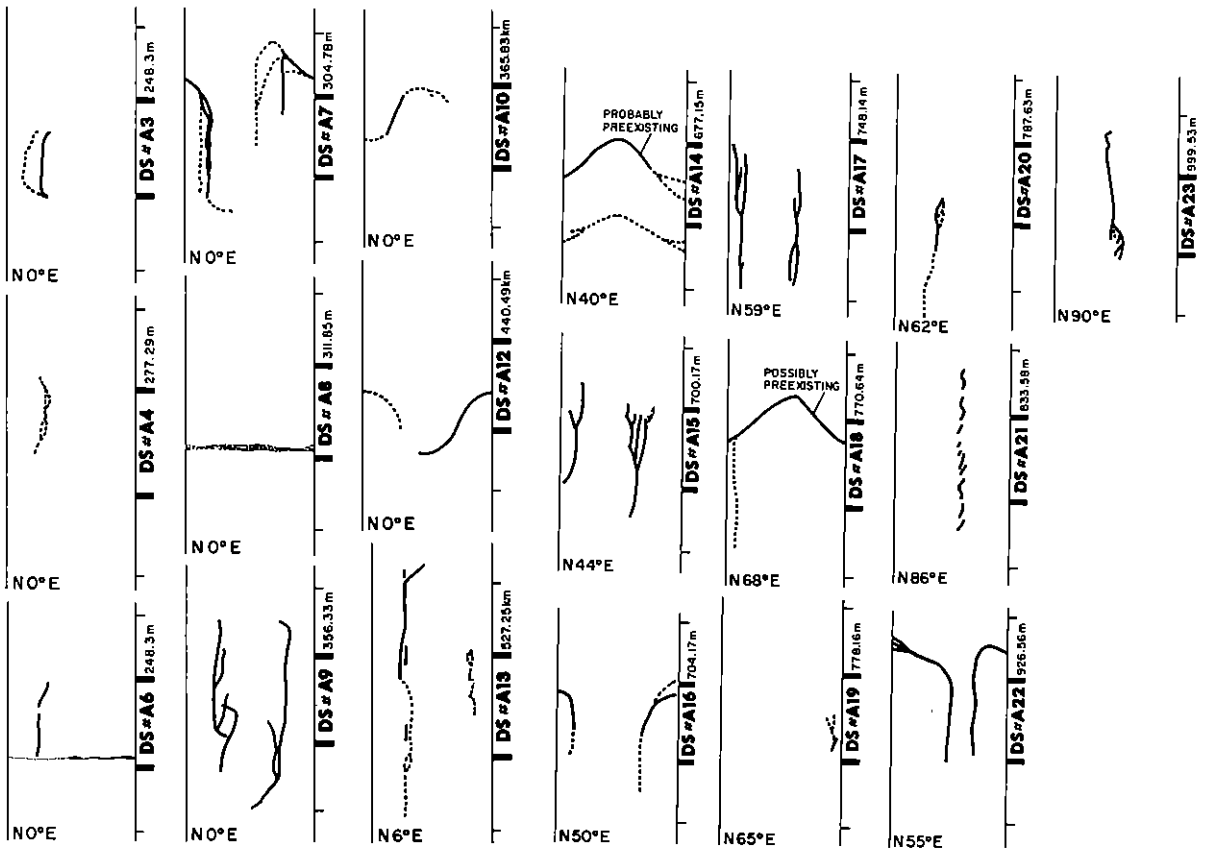

Fig. 12. (continued)

vertical stress contours are strongly deflected downward under the valley, mimicking the surface topography (although less so at depth), whereas the valley-normal horizontal stress contours below 200 m are only slightly perturbed. The valley-parallel horizontal stress magnitudes are given by the plane strain relation $\sigma_y = \nu(\sigma_x + \sigma_v)$. Hence these contours (not shown) are also deflected downward but by a small fraction of the deflection to the vertical stress. For more complicated three-dimensional topography, such as applies to the study area (Figure 2), it is reasonable to infer on the basis of the plane strain model results that topographically induced lateral variations in horizontal stress are a fraction of the corresponding variation in vertical stress. Thus, if the measured ISIPs indeed represent horizontal stresses and all other stress field "components" which augment the modeled gravitational stresses are laterally uniform, then ISIPs measured in different wells at the same stratigraphic level should be similar or, at most, differ by only a small fraction of the overburden difference in the wells. By "overburden" we mean simply ρgd, where ρ is the bulk density of the rock and d is the depth below the wellhead. Referring to Figures 9 and 10, we find that below the K-sand, where there is no reason to doubt that the ISIPs reflect least horizontal stress, the ISIPs measured at common stratigraphic levels are indeed identical. This lends strong support for the inferences we draw from applying the *Savage et al.* [1985] model and implies that nongravitational horizontal stress components present in the section below the K-sand are, indeed, laterally uniform. In contrast, ISIPs which lie on the near-lithostat trends differ at common stratigraphic levels by an amount which is slightly greater than the overburden difference and hence conform more closely to the spatial variation of vertical stress. We next examine how closely.

The difference between the vertical stress and overburden gradients in the Wilkins well and, to a lesser extent, the Appleton well is significant. Physically, this reflects the fact that in a borehole located on a valley floor (i.e., the Wilkins well), the true vertical stress, such as would be sampled by a pressurized horizontal fracture, will increase with depth at a rate greater than the overburden due to "loading" by the surrounding higher topography. In Figures 16*a* and 16*b* we show a comparison between vertical profiles of the overburden, the vertical stress predicted for the two theoretical topographic profiles featured in Figure 15, and the observed near-lithostat ISIPs, for the Wilkins and Appleton wells, respectively. The correspondence between the predicted vertical stress and the ISIPs for both wells is reasonable considering the limitations of the two-dimensional model in representing the three-dimensional topography of the study area. For the O'Dell well the predicted vertical stress, near-lithostat ISIPs and overburden are essentially coincident. Thus the near-lithostat trends correspond closely to the predicted vertical stress profiles in each well. Consequently, we take ISIPs which fall on these trends to be direct measures of vertical stress and to constitute only lower bounds to the true magnitude of the least horizontal stress. This changes the earlier provisional interpretation of *Evans and Engelder* [1986] in which the ISIPs lying on the near-lithostat trends were taken as exact measures S_h.

Least Horizontal Stress in the Transition Zone

The outstanding feature of ISIPs in the transition zone is that values measured in shales are systematically smaller than those in the sands (Figure 10). In the preceding discussion we have shown that ISIPs in the sands are best

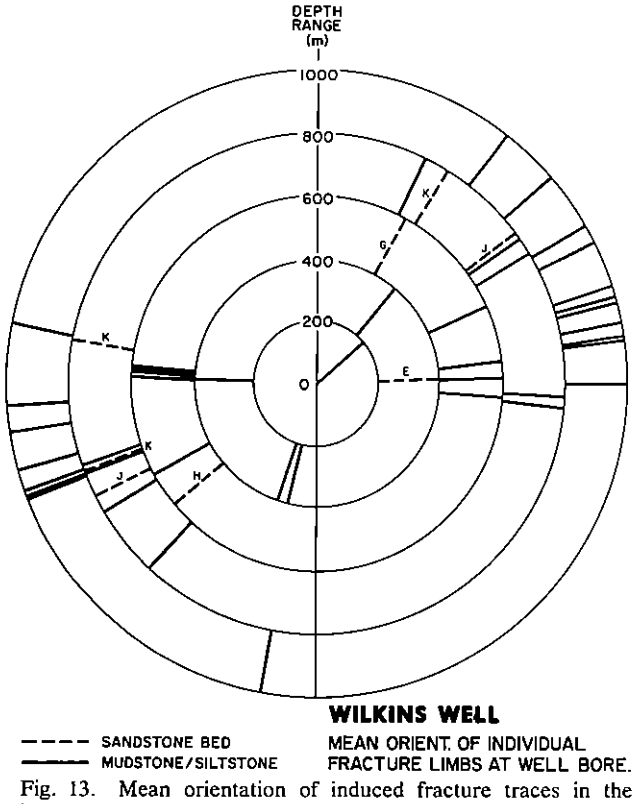

Fig. 13. Mean orientation of induced fracture traces in the Wilkins well in successive depth intervals. The letters identify the specific sand bed. Orientation is specified with respect to true north.

interpreted as measures of vertical stress. Since vertical stress must be a monotonically increasing function of depth, the ISIPs in the shales cannot also be S_v measures. Thus, do they reflect least horizontal stress? We have noted that below the K-sand, ISIPs at common stratigraphic horizons are essentially the same, a result which both supports their interpretation as exact measures of S_h and also implies that nongravitational stress "components" present in the section are essentially laterally uniform on the scale spanned by the wells. Referring to Figure 10, we find that ISIPs recorded in the shale between the J- and K-sands are also fairly well clustered and hence can be taken as reliable measures of S_h. An implication is that least horizontal stress magnitude in the shale undergoes a sudden laterally uniform step change of about 3.5 MPa across the K-sand. Above the J-sands, the shale ISIPs are still significantly less than the level of the vertical stress implied by our analysis. However, they show considerable lateral variation. If they are interpreted as direct measures of S_h, the implication is that for some reason, least horizontal stress (or, rather, its nongravity constituents) does not display the same pattern of lateral uniformity above the J-sand as it does below. Above the G-sand, ISIPs generally fall close to the near-lithostat trends (Figure 9). Thus, if shale ISIPs in the vicinity of the H-sand reflect S_h, then least horizontal stress attains the level of the vertical stress some short distance above the H-sand.

It is worth briefly examining the possible effects of the known bedding-plane weakness of the shale [*Blanton et al.*, 1981] in promoting horizontal fracture-controlled ISIPs (i.e., S_v measures). Near the H-sand in the Wilkins well, shale ISIPs are systematically 1 MPa lower than those of the sands which define the level of S_v (Figure 10). If the shale ISIPs measure S_h, then we must conclude that the presence of bedding-plane weakness did not influence the observed ISIP even though S_v and S_h differed by only 1 MPa. Furthermore, since it is unlikely that the sands exhibit a greater strength anisotropy than the shales, we might also infer that if the induced fractures turned horizontal in the sands during propagation, they did so because S_h in these beds exceeded S_v rather than through exploitation of bedding-plane weakness. A corollary is that ISIPs which fall on the near-lithostat trends can be taken to represent lower bounds to the true magnitude of S_h. The variation in S_h between the sands and shale of the transition zone and between the Tully Limestone and surrounding shales may thus be even greater than the ISIP values plotted in Figures 8–10 suggest.

Maximum Horizontal Principal Stress

Two methods are commonly used to estimate S_H from open-hole hydraulic fracturing data. Both are based upon *Hubbert and Willis*'s [1957] discussion of the mechanics of vertical borehole rupture in the presence of arbitrary far-field horizontal stresses. The first considers the well bore fluid pressure required to induce an axial fracture in a previously unfractured vertical borehole penetrating a uniform, linearly elastic porous medium. Using (implicitly) the fact that for such a medium, the Kirsch solution for the stress concentration about the borehole due to the far-field horizontal stresses is independent of the poroelastic properties of the medium, *Haimson* [1968] derived an expression for calculating S_H from the well bore breakdown pressure P_b which we write given by

$$S_H = 3S_h - P_b + T - P_p^{\text{wall}} + \left\{ \alpha \frac{(1-2\nu)}{(1-\nu)} (P_p^{\text{wall}} - P_p) \right\} \quad (1)$$

Here T is the tensile strength ($T > 0$), P_p is the ambient pore pressure, P_p^{wall} is the pore pressure within the borehole wall at breakdown and α is Biot's constant. The expression is

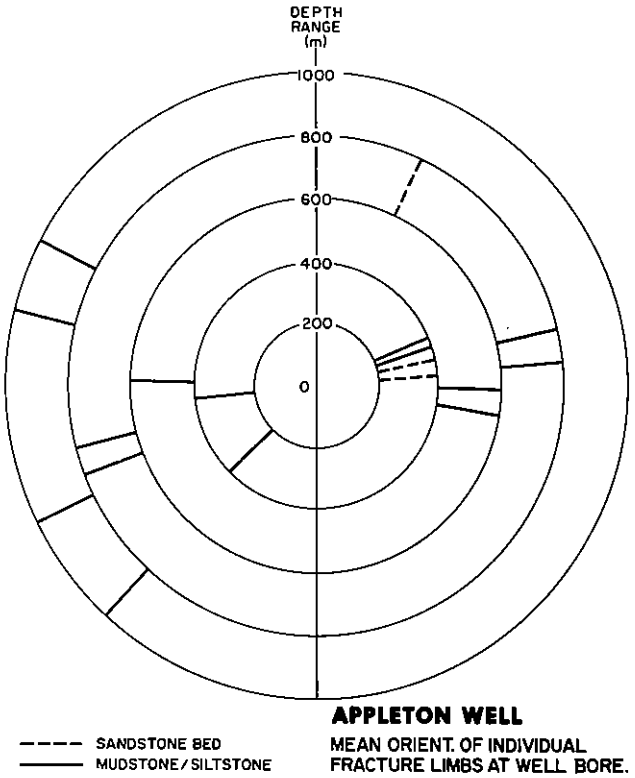

Fig. 14. Mean orientation of induced fractures traces in the Appleton well in successive depth intervals.

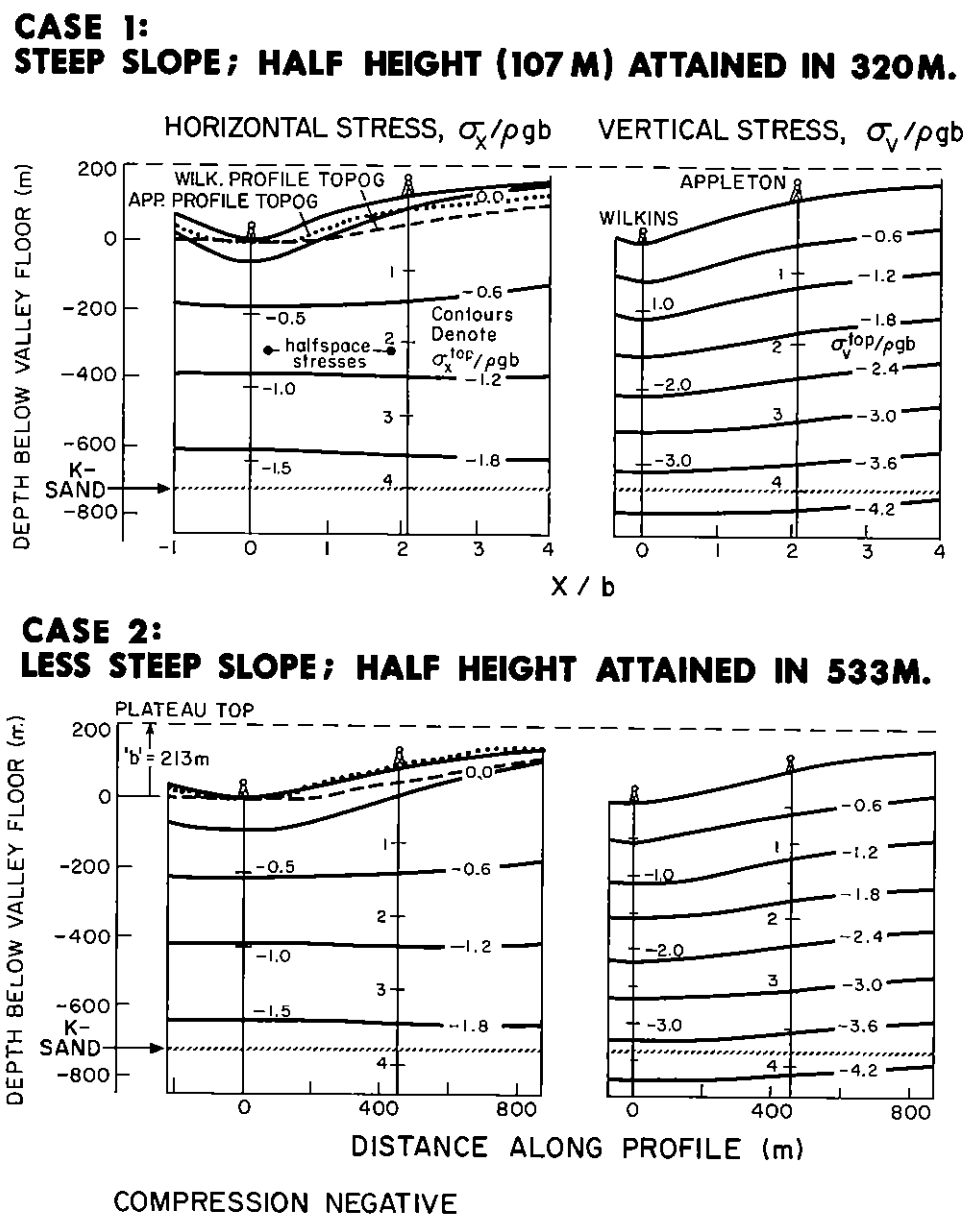

Fig. 15. Contours of (left) horizontal stress and (right) vertical stress predicted to result from the erosion of a symmetric valley into a laterally restrained half-space of Poisson's ratio 0.33. Two topographic profiles are considered. Approximate topographic slopes in the vicinity of the Wilkins and Appleton wells are shown by the dashed and dotted lines, respectively, for comparison with the model slope. All stress magnitudes are normalized to ρgb and must be multiplied by 5.66 to obtain values in megapascals. Horizontal stress magnitudes (left) are essentially laterally uniform at stratigraphic horizons deeper than 300 m below the valley floor. Vertical stress (right) increases with depth below the valley floor at a rate greater than the "overburden" which is delineated for each well by the graduations along the well profile.

exact for two end-member situations. The first is where well bore fluid does not infiltrate the borehole wall during the time taken to raise interval pressure to breakdown levels, and in this case, $P_p^{wall} = P_p$. The second is where significant infiltration occurs such that interval pressure at breakdown extends some considerable distance into the wall. In this case, $P_p^{wall} = P_b$. In view of the submicrodarcy permeability of the majority of rocks in question, we assume infiltration was negligible and take $P_p^{wall} = P_p$. Equation (1) thus reduces to

$$S_H = 3S_h - P_b + T - P_p \quad (2)$$

It is of note that had infiltration been significant, we would expect to observe evidence of horizontal fracture initiation given the inferred stress regime above the H-sand [*Evans et al.*, 1988] yet this was not found. Also *Kalyoncu et al.* [1979] examined core specimens taken from a well 20 km distant from the Canisteo site (EGSP NY1) which sample the same lithologies encountered in the Canisteo wells and reported no detectable permeability. A further demonstration of the remarkably low permeability of these rocks is given by the observation that after a cement plug had been placed in the Appleton and O'Dell wells at the level of the Onondaga

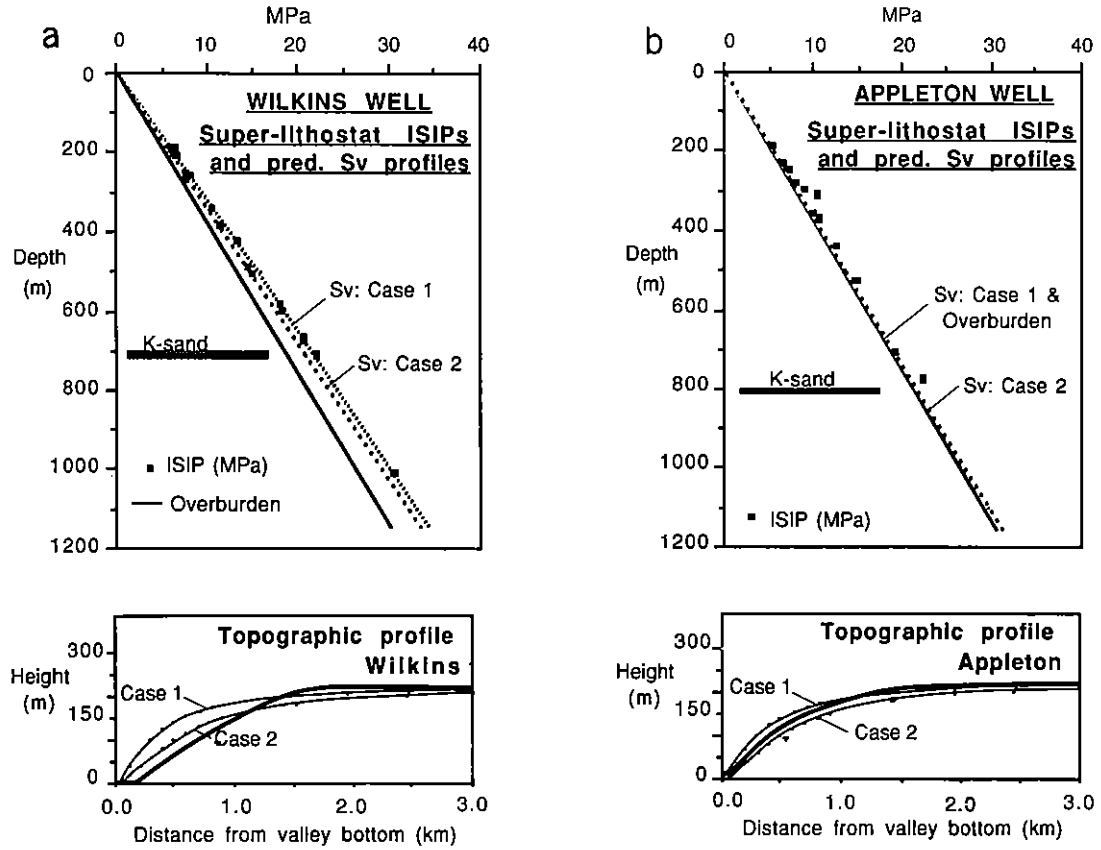

Fig. 16. (*a*) Profiles of vertical stress along the vertical trace of the Wilkins well shown in Figure 15 for the two theoretical topographic profiles considered (shown in the bottom figure). Also shown is the overburden and those ISIPs which define the near-lithostat trends. Evidently, the near-lithostat trends correspond closely with the predicted vertical stress profile. (*b*) Same as Figure 16*a* but for the Appleton well.

limestone (Figure 3) and the water level baled back to 600 m below surface, the level remained stable for 2 years until the wells were refilled with brine several months prior to stress testing. The Wilkins well was loaded with brine some 2 years prior to stress testing.

A drawback with the first method is the necessity to estimate the "appropriate" in situ tensile strength of the rock in question, a requirement which at best can only be fulfilled in a statistical sense [*Ratigan*, 1981]. To overcome this, a second method was suggested by *Bredehoeft et al.* [1976] which considers the well bore pressure required to reopen the fracture induced during the breakdown pump. If it is assumed that the fluid pressure within the fracture near the well bore remains at the level of the formation pore pressure during the pumping period that leads to reopening, the mechanical formulation follows that underlying equation (2) with the exception that the tensile strength term is zero. That is,

$$S_H = 3S_h - P_{RO} - P_p \tag{3}$$

where P_{RO} is the well bore pressure at which the fracture begins to open at the well bore.

Unfortunately, in situations where $S_H > 2S_h - P_p$, method 2 (equation (3)) must be applied with great caution. Where this condition is met, the elastic hoop stress across the mouth of the fracture (in the immediate vicinity of the well bore) is less than S_h. Hence although the fracture may begin to open at the well bore when the true reopening pressure (required by equation (3)) is reached, the "opening" will not propagate beyond the immediate vicinity of the well bore until the pressure reaches the value of S_h, which is the stress normal to the crack face beyond the well bore stress concentration. Unless hydraulically stiff interval pressuring systems are used, the corresponding fluid loss from the well bore may become sufficiently great for detection only when the pressure has reached the value of S_h. In such circumstances, a reopening pressure equal to the ISIP will be recorded, whereas the true reopening pressure that features in equation (3) is less than this. Equation (3) will then yield an underestimate for S_H. In the majority of tests conducted, we observed reopening pressures which were disturbingly similar to the ISIP. The reopen pressures were estimated using the method described by *Hickman and Zoback* [1983]. The hydraulic stiffness of our system is 8.5 MPa/L, a value which is not unusually compliant. However, in view of the possible implications of the correspondence between reopen pressures and ISIPs we have analyzed the data using both methods. Estimates obtained using equation (2) are preferred.

Estimation of pore pressure. For the purpose of calculating S_H estimates from equations (2) and (3) we have assumed that the relevant pore pressure P_p is given by the hydrostatic pressure of the fluid in the well bore (density 1.1 $\times$ 10^3 kg/m^3). Although formation pore pressures in the "Devonian shales" are generally uncertain owing to the difficulty of measurement in rocks of such low permeability, it is the pore pressure in the vicinity of the well bore, rather than the remote formation pressure, that is relevant for

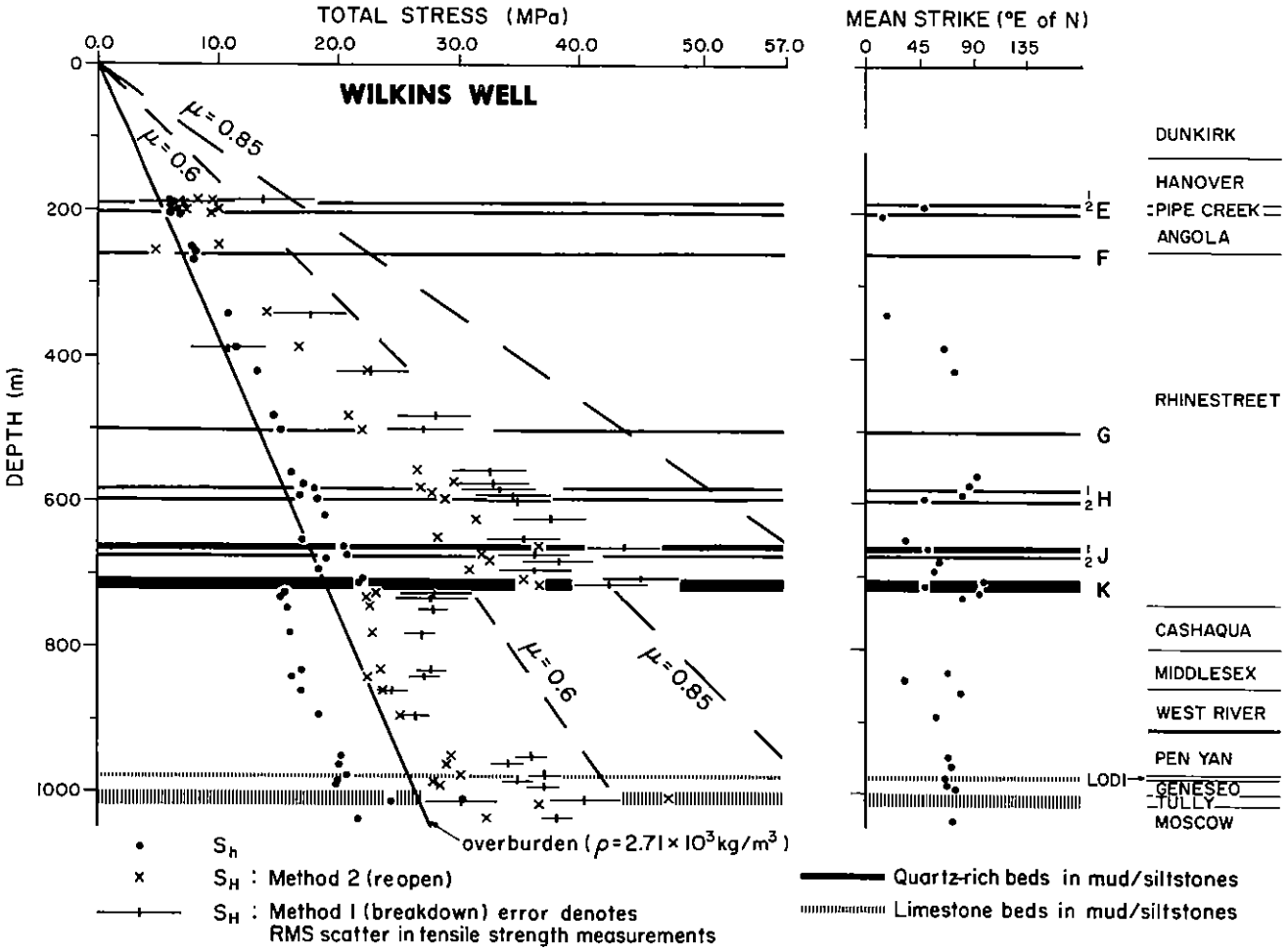

Fig. 17. Summary of total stress estimates for the Wilkins well. The estimates assume that each ISIP is equal to the least horizontal stress at that depth, which is probably untrue in the sands, limestones, and shales above the H-sand. For these beds the estimates shown may be taken correctly as lower bounds to the true values. S_H estimates derived from both "breakdown" (method 1) and "reopening" (method 2) methods are shown. The former are preferred for reasons discussed in the text. The dashed lines denote the S_H thresholds for failure assuming a cohesionless Coulomb failure criterion and hydrostatic pore pressure. The thresholds are shown for two different internal friction angles. The least principal stress is taken as equal to S_v above the K-sand and S_h below.

determining the effective stresses that influence fracture initiation. Mercury porosimetry measurements on core samples from EGSP well NY1 sampling the same shales encountered in the South Canisteo wells yielded values for connected porosity that scatter in the range 0.1–0.01 with a mean value of 0.05 [*Kalyoncu et al.*, 1979]. Hence it is reasonable to assume that fluid pressures within this connected porosity approach equilibrium with well bore pressure, at least in the immediate vicinity of the borehole wall. No mud cake was present to prevent infiltration.

Estimation of tensile strength. The tensile strength values used in implementing method 1 were derived from the tabulated results of oriented Brazilian tests conducted on core samples from the neighboring EGSP well NY1 [*Cliffs Minerals Inc.*, 1981]. Enormous variability was found in the reported data values ranging from 3 to 23 MPa. To reflect this uncertainty, we calculated the statistical mean value and rms standard deviation of the ensemble of values (taken over depth) reported for each stratigraphic group. For the value at each depth we used the smallest of the three tensile strengths measured across planes striking between N30°E and N90°E. This was because the vast majority of the induced fractures were determined to strike ENE. The West Falls Group was particularly well sampled with 81 data suites. The others involved typically 15 test suites. The resultant mean values range between 6.5 and 9 MPa and are similar to those reported by *Blanton et al.* [1981] from direct pull tests conducted on Devonian shales from more central localities of the basin. No measurements were reported for the Tully and Lodi limestones. Hence for these two formations we used a tensile strength value given by Brazilian tests on Indiana limestone of 5.2 MPa reported by *Hardy and Jayaraman* [1970] and have assigned an uncertainty of 3 MPa.

The estimates for S_H derived using the breakdown and reopening methods assuming "well bore" hydrostatic pore pressure are shown for the Wilkins, Appleton, and O'Dell wells in Figures 17, 18, and 19, respectively. No S_H estimates are shown for the deeper measurements in the O'Dell well since we cannot be sure that the malfunction in the downhole tool did not affect the breakdown pressure (unlike ISIP it is not amenable to demonstrations of reproducibility). All estimates plotted assume that the observed ISIP measures S_h, whereas we have shown that those ISIPs which fall on the near-lithostat trends most likely measure S_v and

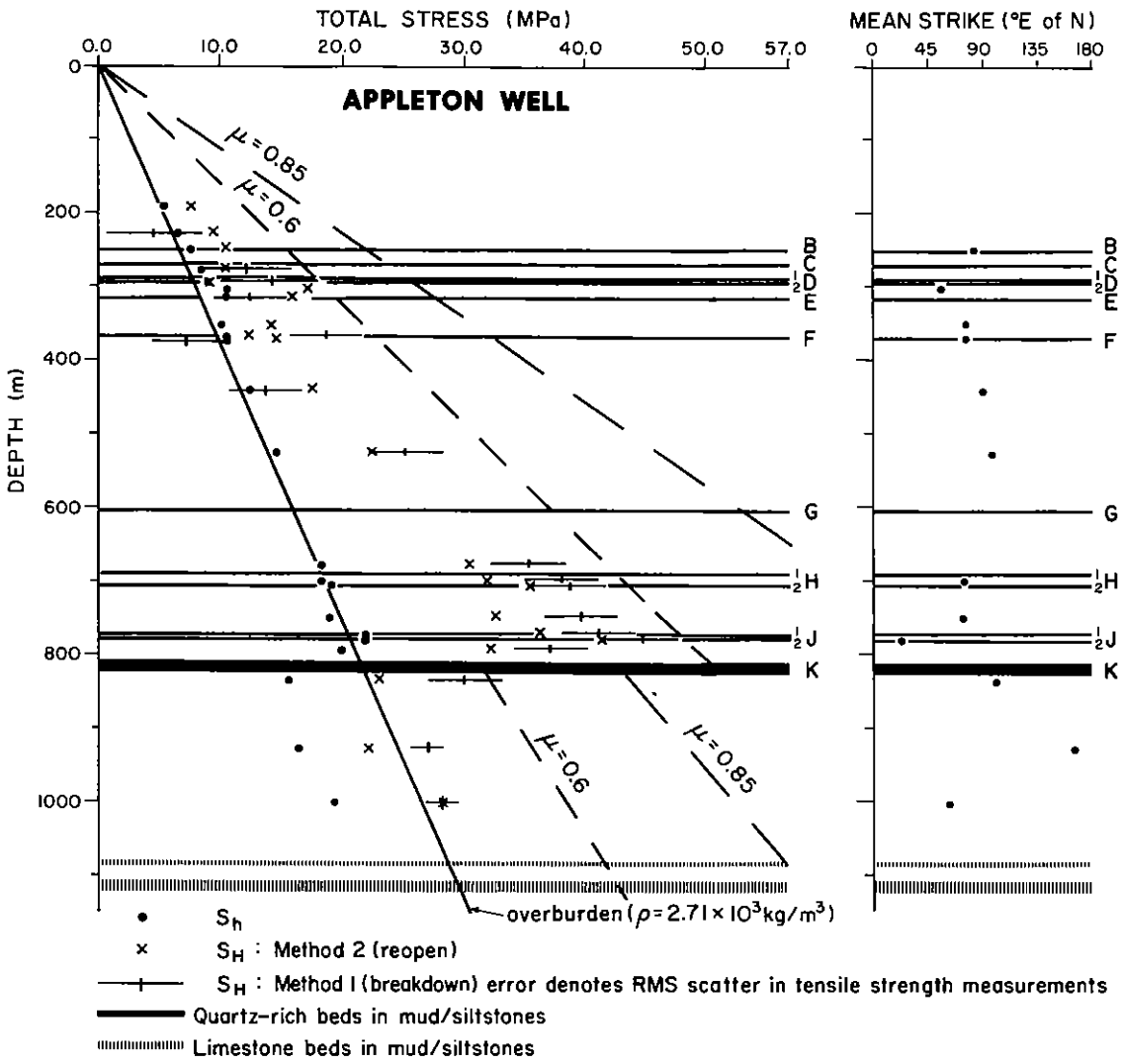

Fig. 18. Summary of total stress estimates for the Appleton well. See Figure 17 for explanation.

provide only lower bounds to the true value of S_h. Where this is the case, the plotted values of S_H must also be taken as lower bounds since from equations 1 and 2 it is clear that the underestimate in S_H will be 3 times that in S_h.

It is evident that estimates derived using method 2 (reopening pressures) are generally less than those derived from method 1 for the reasons discussed previously. A few exceptions are evident which we ascribe to exceptionally high tensile strength of the rock in the straddled interval. Physically unacceptable S_H estimates which are less than S_h are listed in the tables but omitted from the figures. Where such anomalies occur, the lower bound estimate on S_H given by method 2 remains valid. The majority of the high strength intervals were encountered in the shallow sections of the well, and breakdown pressures as much as 30 MPa in excess of reopening pressures were observed. We note that *Haimson and Stahl* [1970] also report similarly high breakdown pressure excesses for tests conducted in neighboring Allegany County at a stratigraphic level equivalent to our B-sand and ascribe them to mud lining the borehole wall. This was not the case here, as mud had never been loaded into any of the holes, all of which were drilled by rotary percussion. Rather, we believe the inferred high tensile strengths are real and reflect locally intact rock of unusually small microcrack size. That the material is capable of such strength is demonstrated by the results of the Brazilian tests where tensile strengths as high as 23 MPa were inferred for some specimens [*Cliffs Minerals Inc.*, 1981].

The S_H profiles show that maximum horizontal stress generally follows the same pattern of variation as the minimum. This is most clear in the stratigraphic superposition shown in Figure 9. Like S_h, the magnitude of S_H in all shales below the J-sand is the same at common stratigraphic levels and undergoes a drop across the K-sand. This drop in S_H between shales above and below the K-sand is 9 MPa, which compares with 3.5 MPa for S_h. The contrast in S_H between the K-sand and the immediately underlying shale is at least 14.5 MPa.

Proximity of Inferred Shear Stress Levels to Coulomb Failure Conditions

In the lower regime, where the horizontal stress estimates are reliable, the ratio between the least and greatest principal stresses is approximately 1.75 to 1. In the upper regime and the transition zone sands, where S_h (and hence S_H) may be underestimated, the ratio is at least 1.75 to 1. Such high levels of shear stress suggest that the shales may be close to failure. To evaluate this possibility, we have calculated the

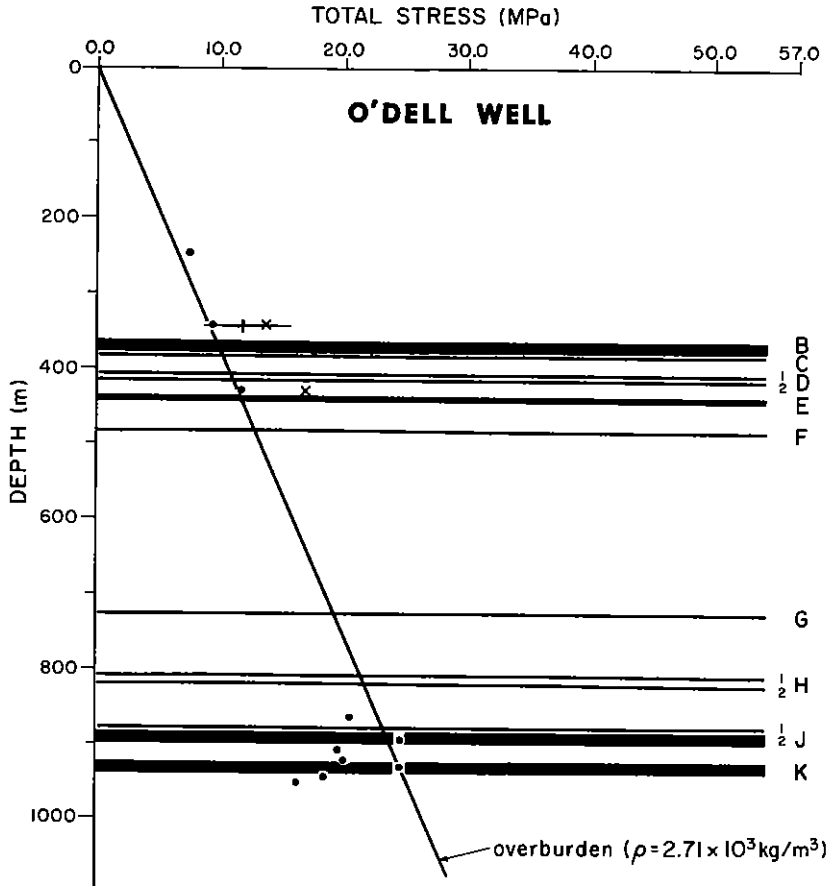

Fig. 19. Summary of stress estimates for the O'Dell well. The estimates assume that each ISIP is equal to the least horizontal stress at that depth.

profile of S_H required for incipient shear failure of a cohesionless Coulomb material supporting the observed S_h and S_v levels and permeated by a hydrostatically pressured pore fluid. We take cohesion as zero for convenience. This assumption will promote underestimation of shear strength, particularly at shallow depths, but it is admissible for our purpose of determining whether the inferred shear stress levels approach plausible failure threshold levels. The critical values of S_H are derived from the equation [e.g., *Jaeger and Cook*, 1976, p. 96],

$$S_1 = S_3 + 2\mu\{(\mu^2 + 1)^{1/2} + \mu\}(S_3 - P_p) \quad (4)$$

where S_1 and S_3 are the greatest and least principal total stresses, P_p is the formation pore pressure, and μ is the coefficient of internal friction. Predicted failure thresholds for both $\mu = 0.85$ and 0.60 are indicated in Figures 17 and 18. For the section above the K-sand (or more precisely, where the ISIP lies on the appropriate near-lithostat trend), the least principal stress is vertical and, neglecting topographic effects, is approximately equal to the overburden ($S_{over} = \rho g d$). Thus we take $S_3 = 26.6d$ MPa where d is depth in kilometers. For the lower regime the least principal stress is horizontal. Here we use $S_3 = 20.5d$ MPa and $S_3 = 19.0d$ MPa to approximate the S_h trends in the Wilkins and Appleton wells, respectively. For shales in the lower regime the threshold S_H levels lie above the observed values for both $\mu = 0.60$ and 0.85. Thus shales in the lower stress regime are not at the point of failure. Consideration of nonzero cohesion would further strengthen this conclusion. For the upper regime the plotted S_H profiles in both the Appleton and Wilkins wells lie close to the failure threshold provided that $\mu = 0.6$. For larger coefficients of internal friction, or the adoption or nonzero cohesion, the predicted threshold would be shifted to values above the plotted S_H estimates. However, as these S_H values can only be taken as lower bounds to the true maximum horizontal stress level, failure conditions might also be met for μ greater than 0.6 and nonzero cohesion. Thus the state of stress in the upper regime, in the transition zone sands, and in the Tully limestone is compatible with view that it is governed by a yield-type behavior which maintains stresses at their limiting value. Since the least principal stress is vertical, the sense of failure is "thrust." The state of stress in the shales of the lower regime, however, is below the limiting value.

Effects of Fracture Propagation Around Packer Seats

Fracturing around packers is a common occurrence during open-hole fracturing operations in shales [*Daneshy et al.*, 1986; *Whitehead et al.*, 1987]. We observed direct evidence of fluid bypass of the packer seals in 18 tests (Table 2). Lower packer bypass was recognized by rushes of fluid uphole during packer depressurization, indicative of a pressurized well bore below. Fluid effusion from the well bore during pumping indicated upper packer bypass. Inspection of televiewer images showed that in all but two of these cases, fracture extension in excess of 0.85 m along the 1.04-m packer seals had occurred (Table 2 and Figure 12). Furthermore, in the Wilkins well a further eight intervals

showed fracture extensions which were sufficient to constitute a potential breach of seal. That no direct evidence was observed in these cases can be partially ascribed to the uncertainty in interval location on the televiewer images (which we suggest is less than 40 cm at 1 km depth).

The section below the K-sand interval was particularly prone to fracture propagation around the packer seal. In fact, all but two Wilkins well tests in this section showed either direct (unequivocal) or televiewer (equivocal) evidence of seal breach (Table 2). As this section corresponds to the lowermost stress regime, it is important to determine whether the low ISIP values which characterize this zone are merely a consequence of seal breach. The following summarized observations testify that the observed ISIP values are indeed valid indications of S_h.

1. The three lowermost tests in the Appleton well showed no evidence whatsoever of bypass and are thus considered valid. These serve to define the existence of the stress transition in the vicinity of the Appleton well at least. The ISIPs for these three Appleton tests correspond closely with values measured at equivalent stratigraphic horizons in the Wilkins and O'Dell wells, a pattern that is consistent with the predictions of simple models of stress fields arising from topographic [*Savage et al.*, 1985] and tectonic [*Savage and Swolfs*, 1986] loading. This suggests the ISIPs do indeed measure S_h despite evidence of bypass in the Wilkins and O'Dell tests.

2. Bypass clearly occurred in a few shallower tests in the Wilkins and Appleton wells. If the ISIPs observed in the deeper Wilkins tests were substantially reduced below true S_h levels because of the existence of a highly conductive fracture path between the interval and the underlying hydrostatically pressured well bore, we would expect to see a similar ISIP reduction in these shallower tests. Two such tests are at 342 and 420 m in the Wilkins well. From Figure 8 it is evident that the ISIPs fall on the same superlithostatic trend defined by neighboring tests for which fracturing was contained within the interval. Thus we infer that the ISIP for these two tests is unaffected by the breach of seal and is a valid indicator of S_h.

3. The shut-in values measured in the lower stress regime define a clear quasi-linear trend which does not correlate with variations in packer setting pressure (Table 2).

4. Tests conducted in the transition zone were largely free of fracture seal breach. The only exception, the J1-sand test in the Wilkins well, showed an ISIP which is consistent with the pattern of stress variations in this zone.

These points serve to establish, albeit empirically, that instantaneous shut-in pressures are not largely affected by fracture propagation around the packer seal, at least in our small volume tests. This would also seem to suggest that in small-volume tests, the observed ISIP is largely determined by the fracture pressure distribution existing within essentially 1 m vertically of the fracture interval. Thus the fracture acts in the manner of an efficient valve which opens when the interval pressure closely approaches the stress normal to the plane of the fracture. *Daneshy et al.* [1986] have presented data from larger-volume injections that lead to similar conclusions.

The quartz-rich beds in which we measured stress contrasts are of the order of only 7–15 m in thickness (Figure 5). In resolving stress in such thin beds we feel it is crucial that fracture dimensions are kept small and injection rates modest so as to avoid overpressuring the fracture resulting in closure stress curves of the form discussed by *Whitehead et al.* [1986]. This is perhaps most important where neighboring beds host higher S_h levels than the test interval, which will serve to limit vertical fracture growth and promote higher fluid pressure excess in the fracture over the local value of S_h in the vicinity of the test interval. Small-volume injections with drainage between pump cycles would seem to have advantage in this regard.

CONCLUSION

Horizontal stresses in the shales undergo a major transition in magnitude at a stratigraphic level which is coincident with a group of sand beds near the base of the Rhinestreet shale. The principal drop occurs across the lowermost sand bed, the K-sand, and corresponds to an offset in S_h and S_H of 3.5 and 9 MPa, respectively. Above the group of sands, least horizontal stress in the shales is at least as great as the vertical stress. We define this as the upper stress regime. Below the group of sands, S_h is significantly less than the vertical stress and is the same at common stratigraphic levels in each well.

Least horizontal stress magnitude in the sands and the Tully limestone is at least as great as S_v. Since S_h levels in the shales decline across the lower sand group, contrasts in stress between these beds and neighboring shales become pronounced with depth. The contrast in S_h between the K-sand and the immediately underlying shale is at least 6 MPa. The corresponding contrast in S_H is at least 14.5 MPa.

The orientation of maximum principal stress as determined from induced fracture orientation is approximately ENE throughout the section. This orientation is in agreement with the midcontinent stress field as mapped by *Sbar and Sykes* [1973], *Zoback and Zoback* [1980], and *Plumb and Cox* [1987]. Although induced fractures were typically splayed and showed considerable scatter in mean orientation (standard deviation of 20°), no systematic correlation with lithology or the major offset in shale stress was evident.

Estimates of S_H obtained using the fracture reopening method are systematically lower than those obtained from the breakdown method. This is not due to incomplete fracture drainage but rather reflects the practical difficulties of determining the appropriate reopening pressure when $S_H > 2S_h - P_p$.

ISIPs appear to have remained unaffected by fracture extension along the length of the packer seals. An implication is that instantaneous shut-in pressures were determined largely by the fracture-normal total stress within a meter or two of the fracturing interval. This result may hold only for small-volume tests as were conducted in this study.

Acknowledgments. This work was supported under DOE contract DE-AC21-83MC20337 with contributing support from Schlumberger-Doll Research (SDR), Exxon Production Research (EPR), and institutional (LDGO) funds. We gratefully acknowledge the initiating support of C. Komar (DOE), C. Shaunessey and L. Lacy (EPR), and C. B. Raleigh (LDGO). We are grateful to Vandermark Associates for permission to utilize their wells and to A. Van Tyne for providing useful unpublished information. We thank R. N. Anderson and Dan Moos for providing access to Ocean Drilling Project televiewers and W. Savage (USGS) for providing a copy of the topographic stress modeling program. Technical support was provided by T. Koczynski and vital field support by Pat Barnes, Greg Boitnott, John Barry, Irene Meglis, Chuck Rine, and Dave

Stocker. Kazuko Nagao drafted the figures. The manuscript benefited greatly from reviews by Fran Boler, Ron Bruhn (Associate Editor), Jack Healy, Chris Scholz, N. Yoshioko, and an anonymous JGR reviewer. Lamont-Doherty Geological Observatory contribution 4438.

REFERENCES

Becker, A., P. Blumling, and W. H. Muller, Recent stress field and neotectonics in the Eastern Jura Mountains, Switzerland, *Tectonophysics*, *135*, 277–288, 1987.

Blanton, T. L., S. A. Dischler, and N. C. Patti, Mechanical properties of Devonian shales from the Appalachian basin, final report to U.S. Dep. of Energy under contract DE-AM21-78MC08216, Morgantown Energy Technol. Cent., Morgantown, W. Va., 1981.

Bredehoeft, J. D., R. G. Wolff, W. S. Keyes, and E. Shuter, Hydraulic fracturing to determine the regional in-situ stress field in the Piceance basin, Colorado, *Geol. Soc. Am. Bull.*, *87*, 250–258, 1976.

Cliffs Minerals Inc., Preliminary laboratory results from EGSP well NY#1-Allegany County, Phase 2 report to U.S. Dep. of Energy under contract DE-AC21-80MC14693, Morgantown Energy Technol. Cent., Morgantown, W. Va., 1980.

Cliffs Minerals Inc., Summary of laboratory analyses and mechanical characterization results for EGSP well NY#1, Phase 3 report to U.S. Dep. of Energy under contract DE-AC21-80MC14693, Morgantown Energy Technol. Cent., Morgantown, W. Va., 1981.

Daneshy, A. A., G. L. Slusher, P. T. Chisolm, and D. A. Magee, In-situ stress measurements during drilling, *J. Pet. Technol.*, *38*, 891–898, 1986.

Davis, D. M., and T. Engelder, The role of salt in fold and thrust belts, *Tectonophysics*, *119*, 67–88, 1985.

Ettensohn, F. R., The Catskill delta complex and the Acadian orogeny: A model, *Spec. Pap. Geol. Soc. Am.*, *201*, 39–49, 1985.

Evans, K. F., A laboratory study of two straddle-packer systems under simulated hydrofrac stress-measurement conditions, *J. Energy Resour. Technol.*, *109*, 180–190, 1987.

Evans, K. F., Appalachian stress study, 3, Regional scale stress variations and their relation to structure and contemporary tectonics, *J. Geophys. Res*, in press, 1989.

Evans, K. F., and T. Engelder, A study of stress in Devonian shale, part 1, 3D stress mapping using a wireline microfrac system, paper presented at 61st Annual Technology Conference and Exhibition, Soc. of Pet. Eng., New Orleans, La., Oct. 5–8, 1986.

Evans, K. F., and T. Engelder, A study of stress in Devonian shales of the Appalachian Plateau, final report to U.S. Dep. of Energy under contract DE-AC21-83MC20337, Morgantown Energy Technol. Cent., Morgantown, W. Va., 1987.

Evans, K. F., and T. Engelder, Some problems in estimating horizontal stress magnitudes in 'thrust' regimes, *Int. J. Rock Mech. Min. Sci. Geomech. Abstr.*, in press, 1989.

Evans, K. F., C. H. Scholz, and T. Engelder, An analysis of horizontal fracture initiation during hydrofrac stress measurements in granite at North Conway, New Hampshire, *Geophys. J.*, *93*, 251–264, 1988.

Evans, K. F., G. Oertel, and T. Engelder, Appalachian stress study, 2, Analysis of Devonian shale core: Some implications for the nature of contemporary stress variations and Alleghanian deformation in Devonian rocks, *J. Geophys. Res.*, this issue.

Frisinger, M., and R. E. Cooper, Techniques for quantifying formation stress and fracture fluid response for optimum hydraulic fracture design, paper SPE 14015 presented at Offshore Europe 85 Conference, Soc. of Pet. Eng., Scotland, Sept. 10–13, 1985.

Gronseth, J. M., and P. R. Kry, Instantaneous shut-in pressures and its relationship to the minimum in-situ stress, in *Hydraulic Fracturing Stress Measurements, Proceedings of U.S.G.S. Workshop XVII, December 2–5, 1981, Carmel, California*, pp. 55–60, National Academy Press, Washington, D. C., 1983.

Haimson, B. C., Hydraulic fracturing in porous and non-porous rock and its potential for determining in-situ stresses at great depth, Ph.D. thesis, Univ. of Minn. at Minneapolis-St. Paul, 1968.

Haimson, B. C., and C. F. Lee, Hydrofracture stress determinations at Darlington Ontario, in *Underground Rock Engineering*, pp. 42–50, Canadian Institute of Mining, Ottawa, Ont., 1980.

Haimson, B. C., and F. Rummel, Hydrofracture stress measurements at the Iceland Research Project drill hole at Reydarfjordur, Iceland, *J. Geophys. Res.*, *87*, 6631–6649, 1982.

Haimson, B. C., and E. J. Stahl, Hydraulic fracturing and the extraction of minerals through wells, paper presented at 3rd Symposium on Salt, N. Ohio Geol. Soc., Cleveland, Ohio, 1970.

Hardy, H. R., and N. I. Jayaraman, An investigation of methods for the determination of tensile strength of rock, paper presented at 2nd International Congress, Int. Soc. of Rock Mech., Belgrade, Yugoslavia, 1970.

Hickman, S., and M. D. Zoback, The interpretation of hydraulic fracturing pressure-time data for in-situ stress determination, in *Hydraulic Fracturing Stress Measurements, Proceedings of U.S.G.S. Workshop XVII, December 2–5, 1981, Carmel, California*, pp. 44–54, National Academy Press, Washington, D. C., 1983.

Hubbert, M. K., and D. G. Willis, Mechanics of hydraulic fracturing, *Trans. Am. Inst. Min. Metall. Pet. Eng.*, *210*, 153–166, 1957.

Jaeger, J. C., and N. G. W. Cook, *Fundamentals of Rock Mechanics*, 2nd ed, John Wiley, New York, 1976.

Kalyoncu, R. S., J. P. Boyer, and M. J. Snyder, Devonian shales: An in-depth analysis of well NY#1 with respect to shale characterization, hydrocarbon content and wire-log data, paper presented at 3rd Eastern Gas Shales Project Symposium, Dep. of Energy, Morgantown, W. Va., Oct. 1–3, 1979.

Kry, P. R., and J. M. Gronseth, In situ stresses and hydraulic fracturing in a deep basin, paper presented at 33 Annual Technology Meeting, Pet. Soc. of Can. Inst. of Min., Calgary, Alberta, June 6–9, 1982.

Lacy, L. L., Comparison of hydraulic-fracture orientation techniques, *Form. Eval.*, *2*, 66–76, 1987.

Mardia, L., *The Statistics of Orientation Data*, 357 pp., Academic, San Diego, Calif., 1972.

Martna, J., R. Hiltscher, and K. Ingevald, Geology and rock stresses in deep boreholes at Forsmark in Sweden, paper presented at 5th Congress, Int. Soc. of Rock Mech., Melbourne, Australia, 1983.

Overbey, W. K., and R. L. Rough, Surface studies predict orientation of induced formation fractures, *Prod. Mon.*, *32*, 16–19, 1968.

Plumb, R. A., and J. Cox, Stress directions in eastern North America determined to 4.5 km from borehole elongation measurement, *J. Geophys. Res.*, *92*, 4805–4816, 1987.

Plumb, R. A., K. F. Evans, and T. Engelder, Correlation of mechanical properties and in-situ stress contrasts (abstract), *Eos Trans. AGU*, *68*, 627, 1987.

Ratigan, J., A statistical fracture mechanics approach to the strength of brittle rock, Ph.D. thesis, 92 pp., Univ. of Calif., Berkeley, 1981.

Rummel, F., J. Baumgartner, and H. L. Alheid, Hydraulic fracturing stress measurements along the eastern boundary of the S-W German Block, in *Hydraulic Fracturing Stress Measurements, Proceedings of U.S.G.S. Workshop XVII, December 2–5, 1981, Carmel, California*, pp. 3–17, National Academy Press, Washington, D. C., 1983.

Savage, W. Z., and H. S. Swolfs, Tectonic and gravitational stresses in long symmetric ridges and valleys, *J. Geophys. Res.*, *91*, 3677–3685, 1986.

Savage, W. Z., H. S. Swolfs, and P. S. Powers, Gravitational stresses in long symmetric ridges and valleys, *Int. J. Rock Mech. Min. Sci. Geomech. Abstr.*, *22*, 291–302, 1985.

Sbar, M. L., and L. R. Sykes, Contemporary compressive stress and seismicity in eastern North America: An example of intraplate tectonics, *Geol. Soc. Am. Bull.*, *84*, 1861–1882, 1973.

Stephansson, O., and P. Ångman, Hydraulic fracturing stress measurements at Forsmark and Stidsvi in Sweden, *Bull. Geol. Soc. Finl.*, *58* (parts 1–2), 307–333, 1986.

Warpinski, N. R., Elastic and viscoelastic calculations of stresses in sedimentary basins, paper SPE 15243 presented at Unconventional Gas Technology Symposium, Soc. of Pet. Eng., Louisville, Ky., May 18–21, 1986.

Warpinski, N. R., S. J. Finley, W. C. Vollendorf, M. O'Brien, and E. Eshom, The interface test series: An in-situ study of factors affecting the containment of hydraulic fractures, *Rep. SAND81-2408*, Sandia Natl. Lab., Albuquerque, N. M., 1982.

Warpinski, N. R., P. Branagan, and R. Wilmer, In-situ stress measurements at DOE's Multiwell Experiment site, Mesa Verde Group, Rifle, CO., paper SPE 12142 presented at 58th Annual

Technical Meeting, Soc. of Pet. Eng., San Francisco, Calif., Oct. 5–8, 1983.
Warren, W. E., and C. W. Smith, In situ stress estimates from hydraulic fracturing and direct observation of crack orientation, *J. Geophys. Res.*, *90*, 6829–6839, 1985.
Whitehead, W. S., E. R. Hunt, and S. A. Holditch, In-situ stresses: A comparison between log-derived values and actual field-measured values in the Travis Peak Formation of east Texas, paper SPE 15209 presented at Unconventional Gas Technology Symposium, Soc. of Pet. Eng., Louisville, Ky., May 18–21, 1986.
Whitehead, W. S., E. R. Hunt, and S. A. Holditch, The effects of lithology and reservoir pressure on the in-situ stresses in the Waskom (Travis Peak) Field, paper SPE 10403 presented at Low Permeability Reservoirs Symposium, Soc. of Pet. Eng./Dep. of Energy, Denver, Colo., May 18–19, 1987.
Zoback, M. D., J. H. Healy, and J. C. Roller, Preliminary stress measurements in Central California using the hydraulic fracturing technique, *Pure Appl. Geophys.*, *115*, 135–152, 1977.
Zoback, M. L., and M. D. Zoback, State of stress in the conterminous United States, *J. Geophys. Res.*, *85*, 6113–6156, 1980.

T. Engelder, Department of Geosciences, Pennsylvania State University, University Park, PA 16802.
K. F. Evans, Lamont-Doherty Geological Observatory, Palisades, NY 10964.
R. A. Plumb, Schlumberger-Doll Research Center, P.O. Box 307, Ridgefield, CT 06877.

(Received November 24, 1987;
revised July 27, 1988;
accepted August 11, 1988.)